© 2016. Published by The Company of Biologists Ltd | Development (2016) 143, 715-727 doi:10.1242/dev.128090

RESEARCH ARTICLE

Molecular model for force production and transmission during vertebrate gastrulation

Katherine Pfister[1,*], David R. Shook[1], Chenbei Chang[2], Ray Keller[1] and Paul Skoglund[1,*]

ABSTRACT

Vertebrate embryos undergo dramatic shape changes at gastrulation that require locally produced and anisotropically applied forces, yet how these forces are produced and transmitted across tissues remains unclear. We show that depletion of myosin regulatory light chain (RLC) levels in the embryo blocks force generation at gastrulation through two distinct mechanisms: destabilizing the myosin II (MII) hexameric complex and inhibiting MII contractility. Molecular dissection of these two mechanisms demonstrates that normal convergence force generation requires MII contractility and we identify a set of molecular phenotypes correlated with both this failure of convergence force generation in explants and of blastopore closure in whole embryos. These include reduced rates of actin movement, alterations in C-cadherin dynamics and a reduction in the number of polarized lamellipodia on intercalating cells. By examining the spatial relationship between C-cadherin and actomyosin we also find evidence for formation of transcellular linear arrays incorporating these proteins that could transmit mediolaterally oriented tensional forces. These data combine to suggest a multistep model to explain how cell intercalation can occur against a force gradient to generate axial extension forces. First, polarized lamellipodia extend mediolaterally and make new C-cadherin-based contacts with neighboring mesodermal cell bodies. Second, lamellipodial flow of actin coalesces into a tension-bearing, MII-contractility-dependent node-and-cable actin network in the cell body cortex. And third, this actomyosin network contracts to generate mediolateral convergence forces in the context of these transcellular arrays.

KEY WORDS: *Xenopus*, Convergence, Extension, Myosin, Cadherin

INTRODUCTION

Gastrulation and elongation of the body axis are key events in shaping vertebrate embryos, but the molecular basis for how the mechanical forces are produced, regulated and propagated across the tissues undergoing this morphogenesis remains incompletely understood. In all vertebrates examined, including frogs (Keller et al., 2000, 1992), fish (Glickman et al., 2003; Solnica-Krezel and Sepich, 2012) and mice (Williams et al., 2014; Yen et al., 2009), the dorsal posterior mesodermal and neural anlage undergo convergence and extension (CE), a narrowing and lengthening of the tissue that occurs by cell intercalation. CE can operate in the context of both mesenchymal and epithelial tissues, and has also been described in developing invertebrate systems, including several distinct regions of the *Drosophila* embryo (Keller, 2006).

[1]Biology Department, University of Virginia, Charlottesville, VA 22903, USA. [2]Department of Cell Biology, University of Alabama, Birmingham, AL 35294, USA.

*Authors for correspondence (kep9v@virginia.edu; paulskog@gmail.com or frogman@virginia.edu)

Received 2 July 2015; Accepted 13 January 2016

In vertebrates, the major cellular process driving CE is mediolateral intercalation behavior (MIB). Initially defined in *Xenopus* (Keller et al., 2000; Shih and Keller, 1992a,b; Wilson and Keller, 1991), MIB-expressing cells become polarized, elongate along the mediolateral axis, and extend large lamelliform and filiform protrusions biased along the mediolateral axis. These protrusions attach to and apply tractional forces to neighboring cells as the cell shortens, pulling cells between one another in support of intercalation. As the cells wedge between one another they generate an extension force of between 0.6 and 5 µN as measured in smaller dorsal tissue isolates or larger whole axial/paraxial explants, respectively (Moore, 1994; Moore et al., 1995; Zhou et al., 2015). The forces generated during *Xenopus* CE are tissue autonomous and internally generated (Keller and Danilchik, 1988). Unlike cells migrating in culture that crawl on a stable substrate, intercalating mesodermal cells act both as force producers and as substrates upon which neighboring cells apply tractional forces. The tensile convergence forces pulling the cells together are thought to be generated by cortical actomyosin structures, either a 'node-and-cable' cytoskeleton or its precursor; this network exhibits contractile oscillations coincident with cycles of cell elongation and shortening (Kim and Davidson, 2011; Rolo et al., 2009; Skoglund et al., 2008). Similar iterated contractile events are associated with a number of morphogenetic processes, including *Caenorhabditis elegans* oocyte polarization (Munro et al., 2004) and in *Drosophila* gastrulation (He et al., 2014; Martin et al., 2009), dorsal closure (Sawyer et al., 2009), germband extension (Fernandez-Gonzalez and Zallen, 2011; Rauzi et al., 2010; Sawyer et al., 2009) and oocyte elongation (He et al., 2010).

Investigations into the molecular basis for embryonic tensional force generation during CE have focused on non-muscle myosin II (MII). MII is a hexameric protein complex consisting of pairs of heavy chains (MIIHCs), regulatory light chains (RLCs) and essential light chains, with three different heavy chains providing MII isoform diversity (Wang et al., 2011). MII complexes exhibit two distinct activities: (1) crosslinking actin filaments to stabilize actomyosin structures and (2) regulated actin- and ATP-dependent contractile activity that slides actin filaments between one another, and that when attached to cellular structures exerts tension (Vicente-Manzanares et al., 2009). Depletion of MIIB in the X*enopus* results in defects in CE, blastopore closure, and development of the node-and-cable actomyosin structures (Rolo et al., 2009; Skoglund et al., 2008), whereas depleting MIIA does not alter CE (Buisson et al., 2014). In the *Xenopus* embryo, MII contractility is likely to be the source of force production in tissues undergoing CE as indicated by characterization of polarized actomyosin structures in these tissues, the presence of mediolateral but not anterior-posterior tension in intercalating cells and small molecule inhibition of MII (Shindo and Wallingford, 2014; Zhou et al., 2009). However, how MII action generates convergence forces, what cellular structures or anchors in the cell are involved in this tension and how these elements function

Development (2016) 143, 715-727 doi:10.1242/dev.128090

in the context of a force-producing intercalation of cells is currently unknown.

During the process of tissue-level convergence, mediolateral tensile forces exerted by intercalating cells during MIB must be transmitted either from cell to cell or through an extracellular matrix (ECM) to form a large-scale, tensile convergence machine stretching across the dorsal, axial mesodermal tissue. Cells exhibiting MIB are surrounded by ECM *in vivo* and MIB is dependent on fibrillin (Skoglund and Keller, 2007), the PCP-dependent deposition of fibronectin at tissue interfaces (Goto et al., 2005) and signaling through the integrin α5β1 receptor (Davidson et al., 2006). Although fibrillin microfibrils are not in the correct geometry to transmit mediolateral tension between intercalating cells (Skoglund et al., 2006), live imaging of fibronectin fibrils reveals remodeling by intercalating cell motility, suggesting that fibronectin fibrils could be used as tractional 'tethers' to transmit tensile force between intercalating cells (Davidson et al., 2004). However, blocking fibronectin fibrillogenesis while leaving the essential fibronectin/integrin signaling intact failed to retard CE (Rozario et al., 2009), suggesting that cell traction on fibronectin fibrils adds little to the force generated by MIB. An alternative idea is that cell intercalation occurs by cell-on-cell traction (Keller et al., 2000, 1992) and this traction could be mediated by calcium-dependent cadherin adhesion (Lee and Gumbiner, 1995). C-cadherin is the predominate cadherin in *Xenopus* tissues undergoing CE and its activity has been shown to be modulated during both CE and mesendoderm migration (Bjerke et al., 2014; Brieher and Gumbiner, 1994; Schwartz and DeSimone, 2008; Zhong et al., 1999).

Here, we examine the consequences of reducing MII contractile activity in the developing embryo. Direct measurements show that convergence force is reduced in explants of the marginal zone and this reduction correlates with failure of blastopore closure in intact embryos. We examine the molecular phenotypes exhibited by intercalating cells experiencing reduced MII contractility, finding defects in both specific actomyosin structures and in the localization of membrane-associated C-cadherin that correlate with this reduction in force production. Observations of the normal dynamics of C-cadherin and actomyosin in cells undergoing CE suggests that they function together to generate and transmit force across the intercalating tissue. Forcing C-cadherin to interact with actin generates physical changes in actin cables, indicating that C-cadherin and actomyosin can functionally interact in the context of these transcellular arrays. These data combine to suggest a model for how actomyosin structures and dynamic cell-cell adhesions can collaborate to generate convergence forces during vertebrate gastrulation.

RESULTS

Development of cadherin adhesions coincides with morphological progression of actin structures

MIB in *Xenopus* deep mesodermal cells is characterized by bipolar protrusive activity and progressive increase of length-to-width ratio with respect to the mediolateral axis. We examined the organization and relative localization of actin and C-cadherin during this process, distinguishing four distinct phases defined by the morphology and dynamics of both cortical actin networks and C-cadherin adhesion structures (Movie 1).

Phase 1 is characterized by an isodiametric cell shape and lamellipodia that are unpolarized with respect to the embryonic axis. C-cadherin and cortical actin are evenly distributed with C-cadherin as a circumferential signal on the cell membrane and actin as a basket around the periphery of the cell (Fig. 1A,E,I). Cells enter phase 2 when they break isodiametric symmetry, first occurring at developmental stage 10.5 by either exhibiting a single large lamellipodial protrusion or extending three or four filopodia in different directions, without respect to the embryonic axis (Fig. 1B,F,J). After 20-30 min in phase 2, the cells adopt the bipolar morphology characterizing phase 3. Cells extend lamellipodia primarily in the medial and lateral directions as they begin to intercalate between neighboring cells. F-actin flowing rearward within lamellipodia coalesces into distal actin structures we call 'proto-nodes' (Fig. 1C, arrowhead) and linear clusters of C-cadherin aligned parallel to the axis of protrusion that colocalize with actin in a similar pattern (20/25 phase 3 cells exhibit both) (Fig. 1G,K, arrows). Several hours later, at stage 12.5, cells begin to exhibit hallmarks of phase 4. Transient proto-nodes stabilize into definitive nodes and thick actin cables link the nodes throughout the cortex (21/23 cells; Fig. 1D,H,L,M). Actin cables are organized as a linear array that spans two neighboring intercalating cells (Fig. 1N, Movie 2).

To investigate the function of proto-node contractions (Fig. 1O,O′), we examined the hypothesis that proto-nodes and C-cadherin in the membrane are a mechanical element linking the actin networks of neighboring cells. We quantified the relative mediolateral movement between the proto-nodes and C-cadherin at the membrane under three conditions: (1) when one cell contracts locally and its neighbor undergoes a corresponding local relaxation; (2) when two adjacent cells each contract; and (3) when two adjacent cells each relax. We found that the C-cadherin exhibits the fastest rate of displacement (Fig. 1P) and spends the largest percentage of time moving (Fig. 1Q) when one cell locally contracts and its neighbor relaxes. This displacement occurred predominantly towards, rather than away from, a local contraction only when the neighboring cell relaxed (Fig. 1R), suggesting a mechanical cooperation between neighboring cells to drive cell intercalation and CE. An example with one cell contracting (arrow) and a paired relaxation (asterisks) is shown in Fig. 1S,S′ and a pair of cells exhibiting contractions in Fig. 1T,T′. These results indicate that the location and appearance of both actomyosin structures and C-cadherin dynamics are developmentally regulated during CE. Moreover, colocalization of C-cadherin and actomyosin in nascent linear arrays suggests they might function together during MIB.

RLC phosphorylation is required to establish notochordal cell polarity

In order to evaluate the role of myosin II contractility in the cellular transitions exhibited during MIB we depleted myosin RLC from developing *Xenopus* embryos. Morpholino (MO)-mediated knockdown resulted in 50% depletion of RLC protein compared with either control morpholino (COMO)-injected or uninjected embryos (Fig. 2A). To determine whether depleting RLC has functional consequences in the intact embryo, we examined the morphology of mosaically morphant axial cells coinjected with fluorescent dextran. We found that morphant mesodermal cells appeared disorganized and displayed irregular morphologies compared with COMO-injected cells (Fig. 2B,B′), indicating that normal cell morphology depends on normal levels of endogenous RLC in intact embryos. Because this cell shape phenotype is similar to that observed in *Xenopus* notochordal cells morphant for MHC-IIB (Skoglund et al., 2008), we examined the levels of MHC-IIB in RLC morphant embryos. We found that MHC-IIB exhibited RLC MO dose-dependent degradation to generate faster-migrating MHC-IIB fragments when assayed by western blotting (Fig. 2C, arrowheads). In order to rescue this effect, we expressed either a wild-type RLC (wtRLC) or a phospho-null mutant of RLC (T18A;

Development (2016) 143, 715-727 doi:10.1242/dev.128090

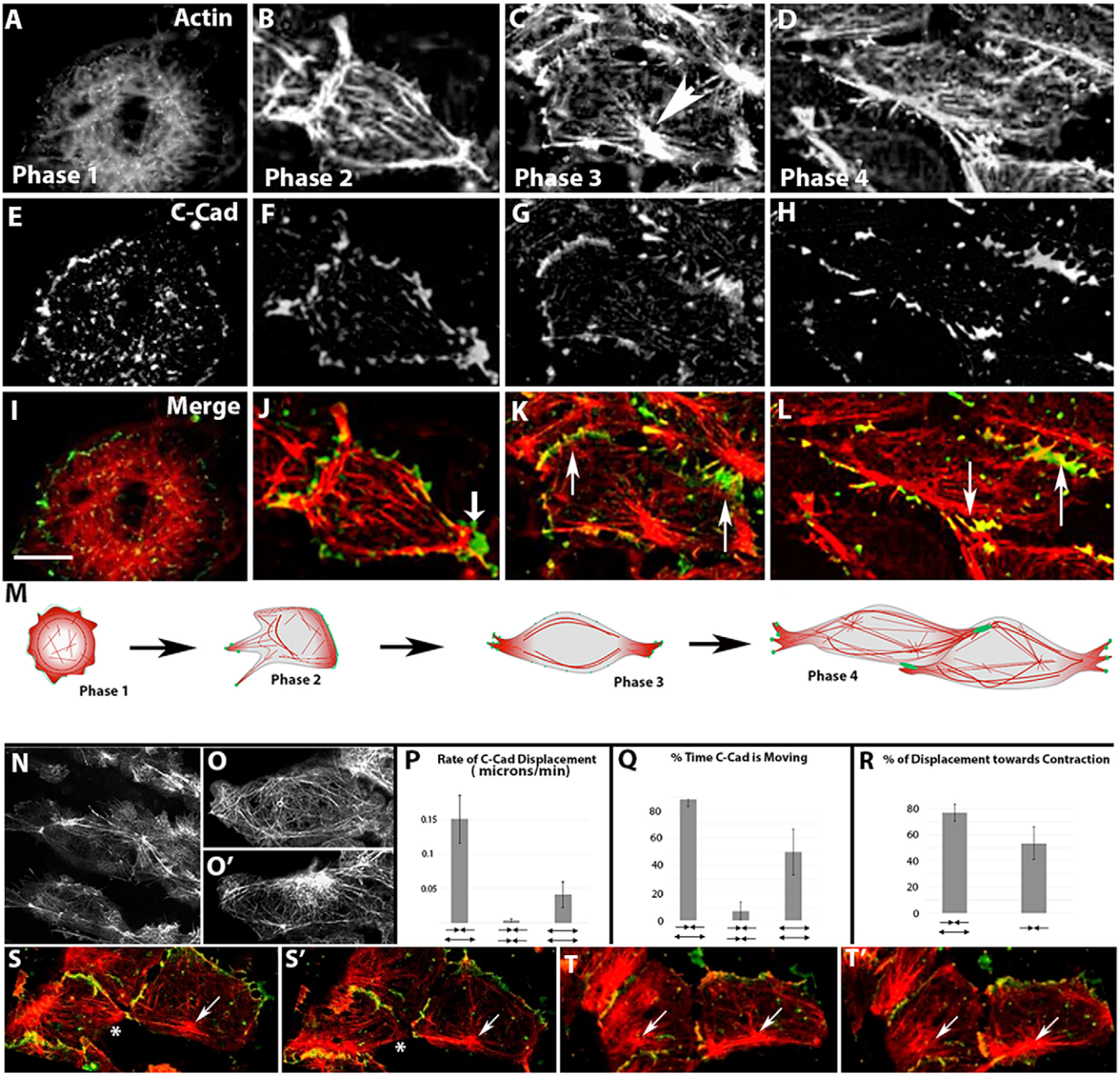

Fig. 1. Actin and C-cadherin dynamics during mediolateral intercalation behavior. Representative images of actin organization (A-D), C-cadherin distribution (E-H) and double-labeling (red, actin; green, C-cadherin) (I-L) in cells in dorsal marginal zone explants during the four phases of MIB (M). Scale bar: 20 µm. (N) Linear arrays of actin spanning multiple cells are seen in a late stage dorsal marginal explant. Node condensation is represented by an increase in fluorescent intensity in an ROI, O′ is 30 s after O. Quantification of rate of mediolateral displacement (P) and time C-cadherin is displaced (Q) in cases where one cell contracts and the neighbor relaxes, when both cells contract or when both cells relax (arrows below bars from left to right, respectively). (R) Proportion of displacement towards a node contraction in the specific cases where one cell contracts and the neighbor relaxes compared with contraction events, regardless of the behavior of the neighbor cell. For P, Q and R, *n* is a minimum of 12 events from 6 cell pairs. Both a contraction (arrow)/relaxation (asterisk) pair (Fig. 1S,S′) and a contraction/contraction pair (arrows) are shown (Fig. 1T,T′).

S19A) (pnRLC) in embryos, both tagged with mCherry (Fig. 2D). Immunofluorescence of cultured axial explants revealed that ∼50% of both MHC-IIB and RLC are depleted in RLC morphant explants, and that this effect could be rescued by expression of either wtRLC or pnRLC (Fig. 2E). This result was also confirmed in whole embryos by using western blotting, with either wtRLC or pnRLC expression restoring MHC-IIB levels in RLC-depleted morphant embryos (Fig. 2F). RLC morphants also exhibited an increased average cell surface area in explants, similar to the whole embryo phenotypes in Fig. 2B, and this phenotype could be rescued by expression of either wtRLC or pnRLC (Fig. 2G). Expression of either wtRLC or pnRLC rescued both MHC-IIB levels in RLC morphants and cell surface area phenotypes, and we therefore conclude that any differences between these two rescue phenotypes allow for direct examination of the role of RLC phosphorylation in the context of the MII complex during CE.

The average length-width ratio of control intercalating cells in late stage CE was ∼3. Scatter-injected RLC morphant cells in the

Development (2016) 143, 715-727 doi:10.1242/dev.128090

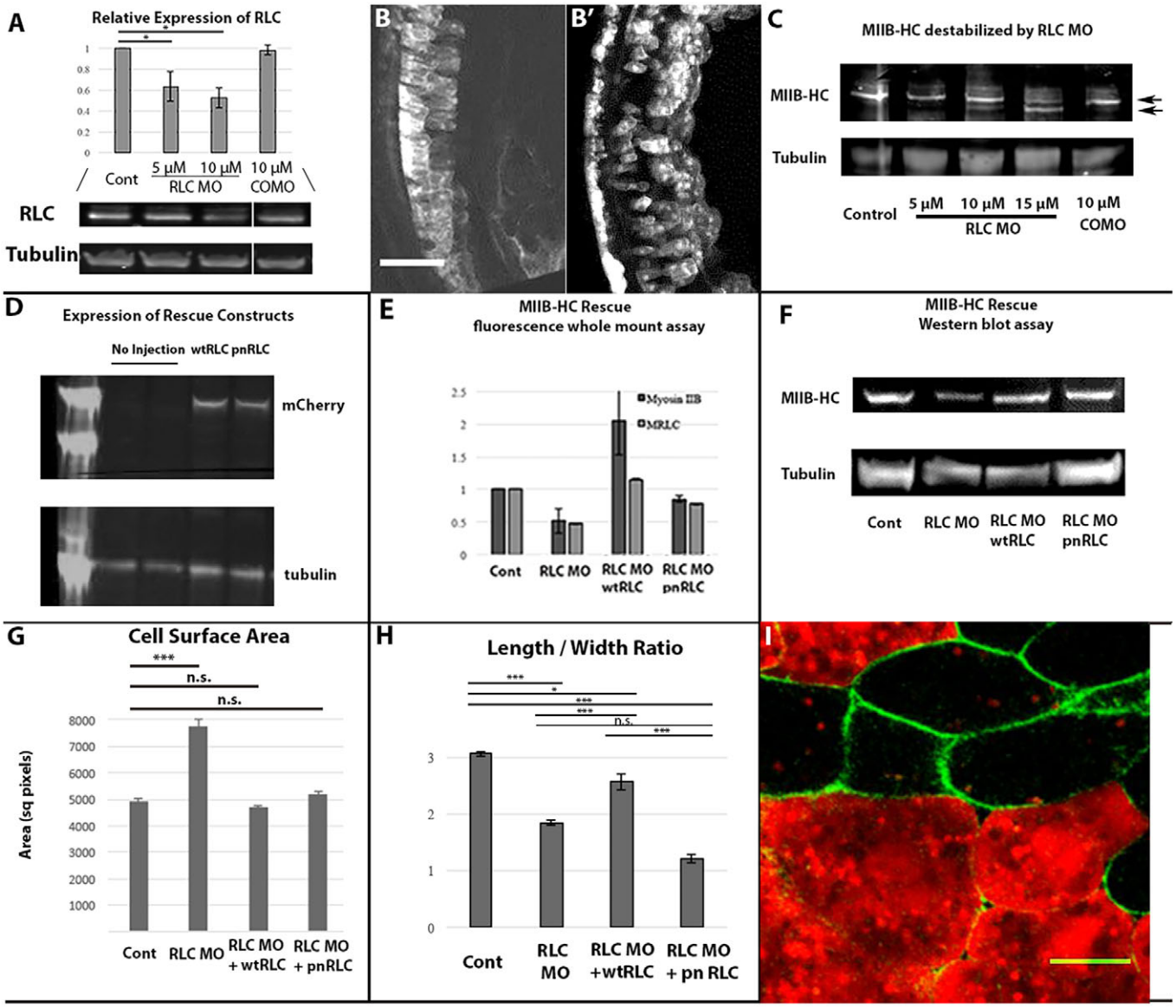

Fig. 2. Regulatory light chain molecular and cellular phenotypes. (A) Western blotting reveals RLC protein decreases in a MO dose-dependent manner compared with COMO (*n*=13 gels). (B) Scattered COMO (B) or RLC morphant (B′) cells in intact stage 17 embryos visualized in 15 µm *Z*-projections of stacks by means of co-injected fluorescent Rhodamine-dextran reveals a cell shape dependence on RLC levels. (C) Myosin IIB heavy chain levels exhibit an RLC MO dose-dependent decrease associated with an increase in proteolytic degradation. (D) Injecting wtRLC-mCherry or pnRLC-mCherry mRNA into developing embryos leads to protein expression as detected by anti-mCherry antibody. (E,F) Two methodologies show that wtRLC and pnRLC expression rescues MHC-IIB stability; quantification of RLC and myosin IIB immunofluorescence levels in RLC morphant dorsal marginal zone explants (E; *n*=7 explants/condition) and western blot analysis of myosin IIB heavy chain levels in RLC MO embryos (F). (G) RLC morphant cells have a larger surface area than control cells in explants and this phenotype can be rescued by either wtRLC or pnRLC expression (*n* is at least 52 cells/condition). (H) However, RLC morphant cells have a reduced length-to-width ratio. Expression of wtRLC but not pnRLC substantially rescued this cell shape phenotype (*n*, at least 14 cells/condition). (I) Morphant cells expressing pnRLC labeled with Rhodamine-dextran (red) display lower length-to-width ratios than corresponding control cells (green). Error bars represent s.e.m. Cont, control. Scale bar: 100 µm in B and 20 µm in I.

context of a wild-type explant displayed an average aspect ratio of <2:1 (Fig. 2H). This cell shape phenotype was rescued by expressing wtRLC, but not pnRLC, indicating that full expression of cell shape polarization during MIB requires normal levels of RLC phosphorylation on T18/S19 (Fig. 2I).

RLC phosphorylation is required to generate convergence force in explants and for morphogenesis in intact embryos

To directly test the hypothesis that RLC phosphorylation is required to generate the forces that drive convergence and extension of dorsal mesoderm, we utilized a biomechanical measuring device termed the ‘tractor pull’ (Fig. 3A). This device measures the cumulative tensional convergence forces developed by pairs of control or morphant marginal zone explants in a ‘giant sandwich’ configuration (Sater et al., 1993; Poznanski and Keller, 1997). We found that explants derived from RLC morphant embryos converged with about 500 nN less force than control explants by the end of gastrulation (Fig. 3B). These tensile pulling forces could be rescued in explants made from RLC morphants rescued with wtRLC, but not by expression of pnRLC, demonstrating that normal convergence forces require the presence of an RLC that can be phosphorylated (Fig. 3C).

Development (2016) 143, 715-727 doi:10.1242/dev.128090

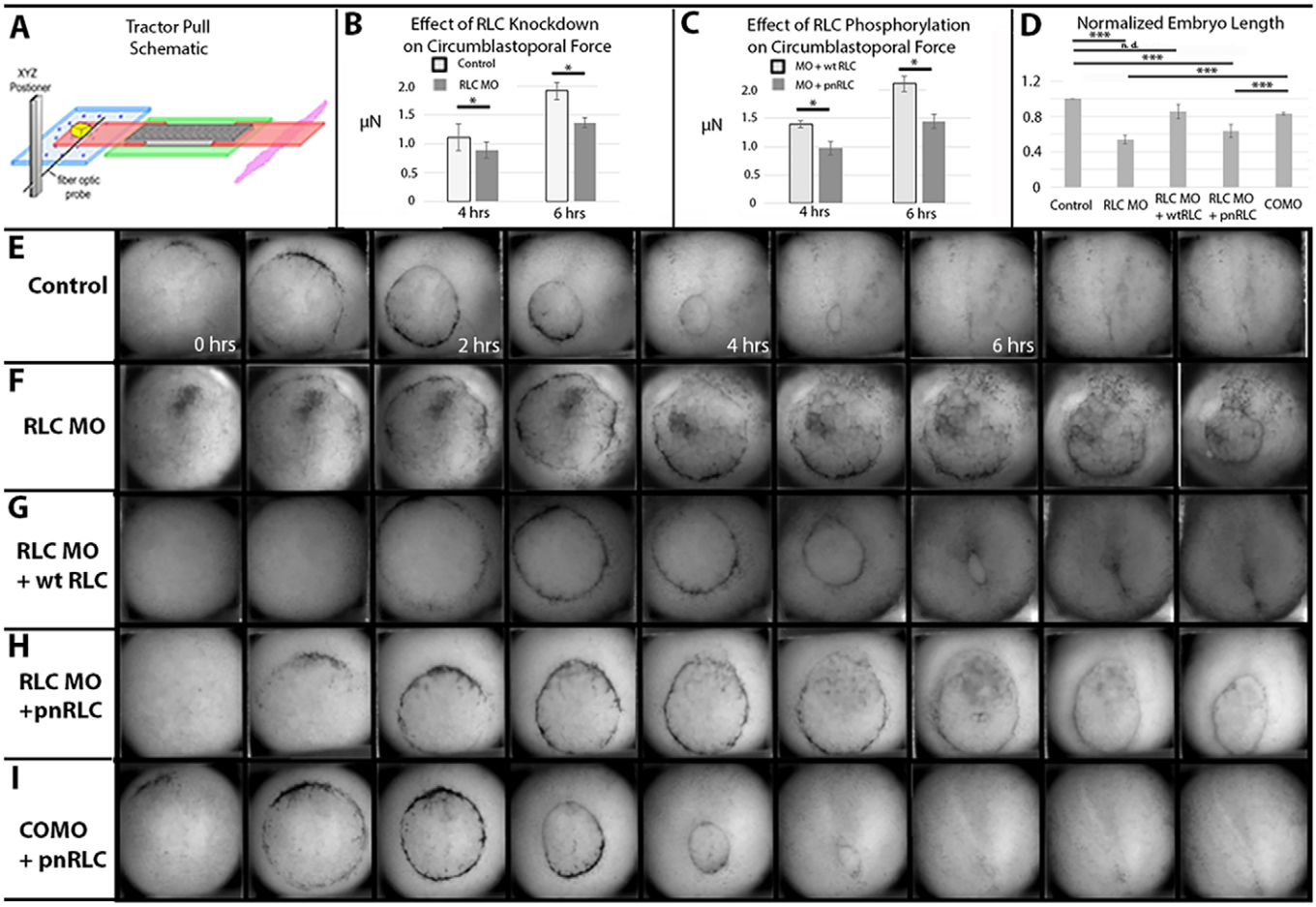

Fig. 3. Reduced convergence forces affect whole embryo morphology. (A) Schematic of the 'tractor-pull' device to measure convergence forces. Explants made from RLC morphant embryos generate less pulling force than controls (B) and co-expressing wtRLC but not pnRLC rescues these pulling forces (C) as measured in sandwich explants at 4 and 6 h after the onset of gastrulation (n=6 axes/condition). (D) The length of tailbud stage embryos is reduced in RLC morphants; this effect is rescued by wtRLC but not pnRLC co-expression (n, at least 9 embryos/condition). (E-I) Time-lapse movies show normal blastopore closure (E), delayed blastopore closure in an RLC morphant (F) and rescue by expressing wtRLC (G). This delay is not rescued by expression of pnRLC (H), although an embryo co-injected with pnRLC and COMO gastrulates normally (I). Times indicate hours post stage 10, and dorsal is up in E-I. *P<0.05, ***P<0.001.

We next examined whether reduced force production in RLC morphant embryos had any overt effect on embryo morphology by measuring embryo length. At control stage 30, RLC morphant embryos were about half the length of control uninjected sibling embryos and 30% shorter than COMO-injected siblings (Fig. 3D). This defect in axial (anterior-posterior) extension can be rescued by wtRLC expression but not pnRLC expression, indicating that axial length in the embryo correlates with the magnitude of tensional convergence forces generated in the dorsal axis during gastrulation. Moreover, both axial elongation and tensile convergence forces depend on phosphorylatable RLC. We also found that blastopore closure was delayed or blocked in RLC morphant embryos (Fig. 3E,F, Movie 3) and this effect could also be rescued by expression of wtRLC but not pnRLC (Fig. 3G,H). We rule out the presence of neomorphic activity arising from expression of pnRLC that might result in failure to rescue morphogenesis because COMO-injected embryos expressing pnRLC closed their blastopores similar to control embryos (Fig. 3H).

Actin movement in cell body nodes and proto-nodes depends on RLC phosphorylation

The progressive maturation of the cortical actin cytoskeleton from isodiametric to a polarized and contractile node-and-cable system was inhibited in RLC-depleted embryos. Although RLC morphant cells maintained a crosslinked actin network throughout this time, they displayed, on average, fewer than one node per cell, compared with control cells that displayed more than three nodes per cell (Fig. 4A,B, Movies 4 and 5). The number of dynamic nodes per cell was partially rescued by wtRLC expression but not by pnRLC expression (Fig. 4C-E, Movies 6 and 7). Actin nodes were previously shown to exhibit mediolaterally polarized movement (Fig. 4F; Kim and Davidson, 2011; Skoglund et al., 2008) and we show here that this movement also depends on normal RLC levels (Fig. 4G). Although the lifetime of nodes was similar in morphant and control cells, the rate of mediolateral movement of nodes in RLC morphant cells decreased and node movement was partially rescued by expression of wtRLC but not pnRLC (Fig. 4H).

We next analyzed the rate of actin flow in control or RLC morphant cells in these explants. A depiction of the kymograph measurements is shown in Fig. 4I. We separated actin flow into two regions of the cell: the lamellipodial protrusions and the cell body cortex containing proto-nodes. Lamellipodial actin flow rates were measured transverse to rearward flow, whereas the radial proto-node condensation actin flow rates were averaged across two axes (red dashed lines in Fig. 4I). RLC depletion significantly decreased the rate of actin flow during condensation of proto-nodes and

Development (2016) 143, 715-727 doi:10.1242/dev.128090

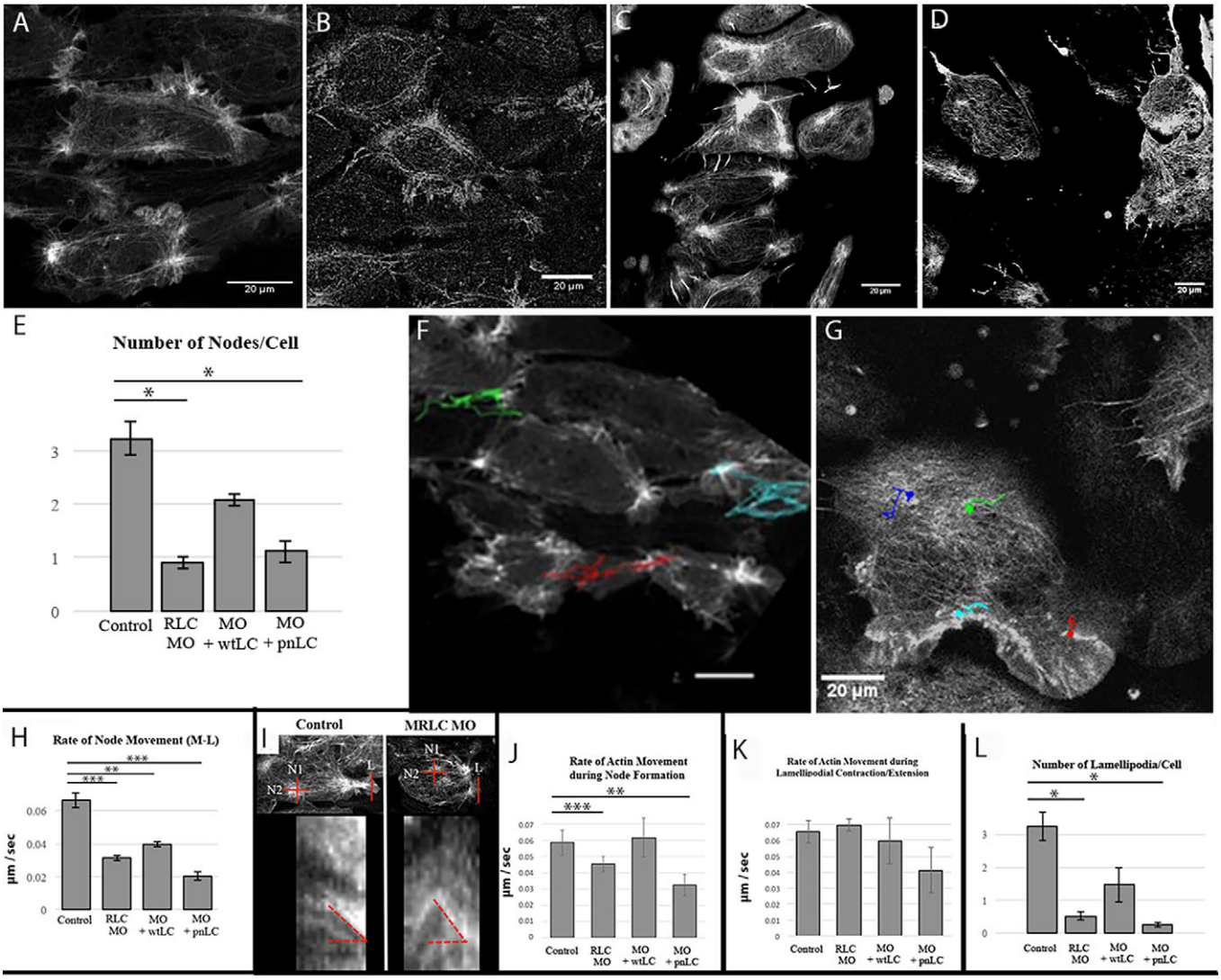

Fig. 4. Actin structures depend on RLC phosphorylation. (A) Imaging of the cortical actin structures in control cells reveals a normal cortical actin structure. (B) An RLC morphant cell exhibits a reorganization of cortical actin. This effect is partially rescued by wtRLC expression (C), but not pnRLC expression (D). (E) These differences are quantified by comparing the number of node structures per cell (*n*, at least 22 cells assayed/condition). Dots represent the starting point of the node and the lines represent the node displacement for a control cell (F) and RLC morphant cell (G) are shown. (H) Rate of node movement (at least 9 nodes assayed per condition). Quantification of kymograph analysis of cortical actin in the regions shown (I), shows a reduction in the rate of actin movement during node formation that depends on RLC phosphorylation (J). (K) By contrast, actin movement in lamellipodia is not sensitive to RLC depletion. For J,K, at least 48 kymographs were averaged for each condition. (L) The number of new lamellipodia per cell also depends on RLC phosphorylation (*n* is at least 31 lamellipodia for each condition). All MOs are at 10 µM. Scale bars: 20 µm. Error bars represent s.e.m. **P*<0.05, ***P*<0.005, ****P*<0.001.

expression of wtRLC, but not pnRLC, restored normal actin network flow rates (Fig. 4J). By contrast, RLC depletion did not affect the rate of lamellipodial F-actin flow (Fig. 4K). However, the number of lamellipodia on these MIB-expressing cells was significantly reduced upon RLC depletion – a phenotype that depends on phosphorylatable RLC (Fig. 4L).

Relationship between transcellular cable components

Double labeling of RLC and actin showed their colocalization in intercalating cells and analysis of relative fluorescent intensities indicated that RLC was evenly distributed across the node-and-cable structure of this actomyosin network (Fig. 5A,B). In whole-mount immunostaining for both MIIB heavy chain and phosphorylated RLC, both MIIB and pnRLC localized to the cell cortex (Fig. 5C). RLC morphant explants exhibited both reduced MIIB and pRLC staining (Fig. 5D), which were both rescued by wtRLC expression (Fig. 5E), whereas only MIIB levels were rescued by pnRLC expression (Fig. 5F).

C-cadherin protein dynamics and localization depend on RLC phosphorylation

Because we hypothesized that C-cadherin serves as the intercellular adhesion protein supporting transcellular tension across the tissue, we examined C-cadherin dynamics in intercalating cells. Immunostaining experiments utilizing an antibody against C-cadherin in explants revealed that the intensity of C-cadherin staining in puncta was reduced in RLC morphant explants at both stage 10 (Fig. 5G,H) and stage 12 (Fig. 5I,J). Live imaging of both red (tdTomato)- and green (GFP)-tagged C-cadherin in neighboring cells in explants revealed that they colocalized at the cell membrane, consistent with a role for C-cadherin in adhesion during gastrulation (Fig. 5K-M) (Lee and Gumbiner, 1995).

Development (2016) 143, 715-727 doi:10.1242/dev.128090

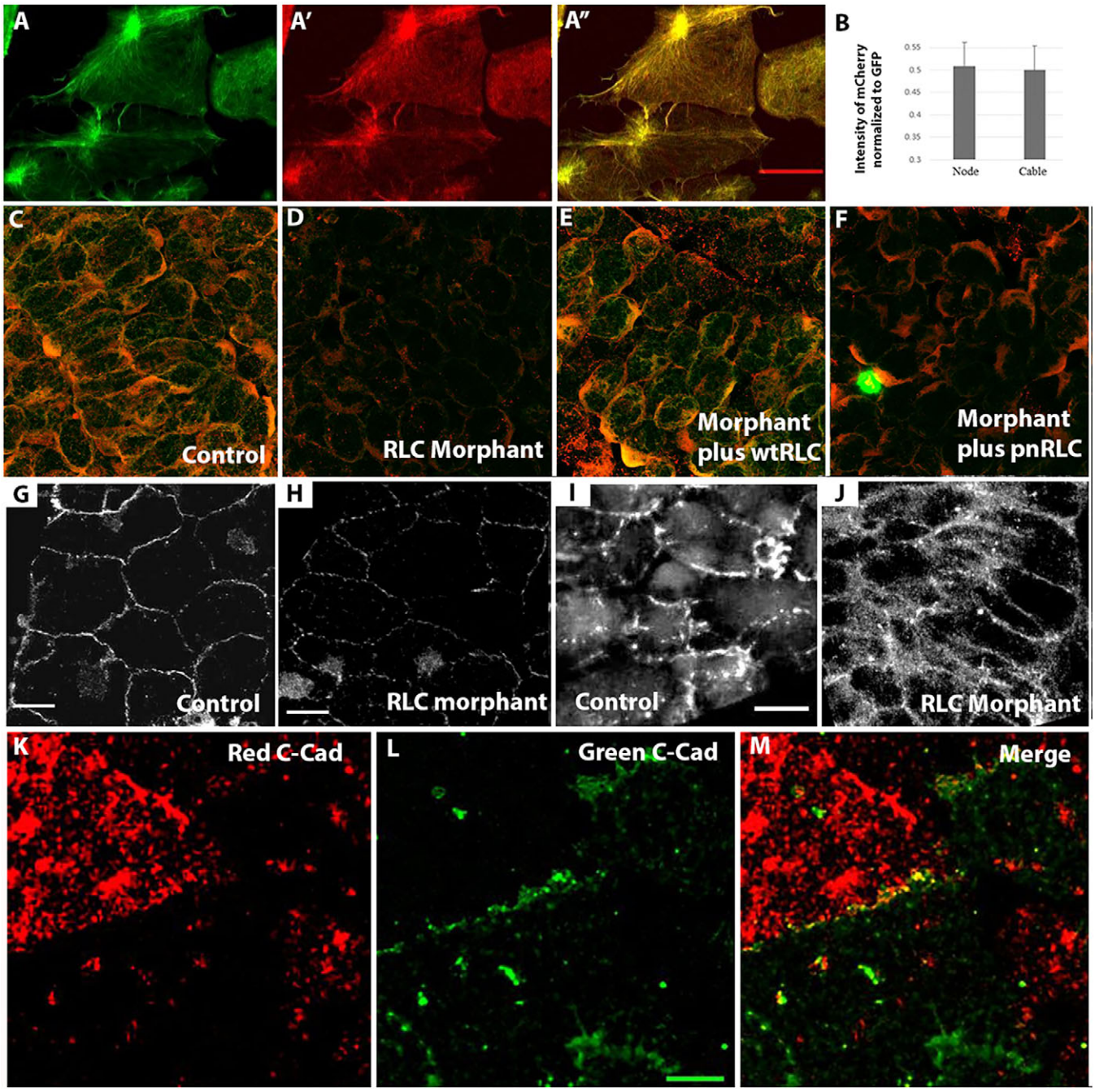

Fig. 5. Colocalization and interdependencies of transcellular array components. (A,B) Imaging of F-actin with moe-GFP (A) and RLC with wtRLC-mCherry (A′) shows colocalization (A″) in both node-and-cable structures with the same relative concentrations in both (B; *n*=8 regions of interest). (C) Both pRLC and MHC localize to cell cortices in stage 13 explants using both MHC-IIB (red) and mono-phosphorylated RLC (green) (S19-P) antibodies. Levels of both are reduced in RLC morphants (D), and rescued by expression of wtRLC (E), whereas pnRLC expression rescues heavy chain IIB but not pRLC levels (F). At both stage 10 (G,H) and stage 12 (I,J), C-cadherin localization by immunostaining is perturbed in RLC morphant cells (H). Expression of red (K)- and green (L)-labeled C-cadherin in neighboring cells reveals that they colocalize at the membrane (yellow in M), as expected if they have a role in adhesion. Scale bars: 20 µm in A*,G-I and 10 µm in L.

C-cadherin in polarized lamellipodia became dynamically associated with active actin extension and rearward flow (Fig. 6A, Movie 8). We found more mature C-cadherin adhesion plaques at the cell boundaries, specifically between linear actomyosin filaments in both cells (Fig. 6B, asterisk). These adhesions moved in concert with actin movements in both cells (Movie 9) and occasionally underwent rapid release and retraction at regions where cells contacted one another, suggesting they are under tension (Fig. 6D, Movie 10). We found 92±26% incidence of these large C-cadherin adhesion plaques per cell in one confocal section, lasting an average of 220±71.75 s (*n*=23 cells). By contrast, C-cadherin signal remained diffuse in lamellipodia of RLC morphant explants and did not often mature into clusters of cadherin plaques (Fig. 6C, Movie 11). There was a 23±8% incidence per cell of these adhesions, which were on average 70% smaller and lasted on average 18±5.5 s (*n*=61 cells). The dynamic behavior of C-cadherin at presumptive sites of cell-cell contact differed in RLC morphants compared with that in COMO-treated

Development (2016) 143, 715-727 doi:10.1242/dev.128090

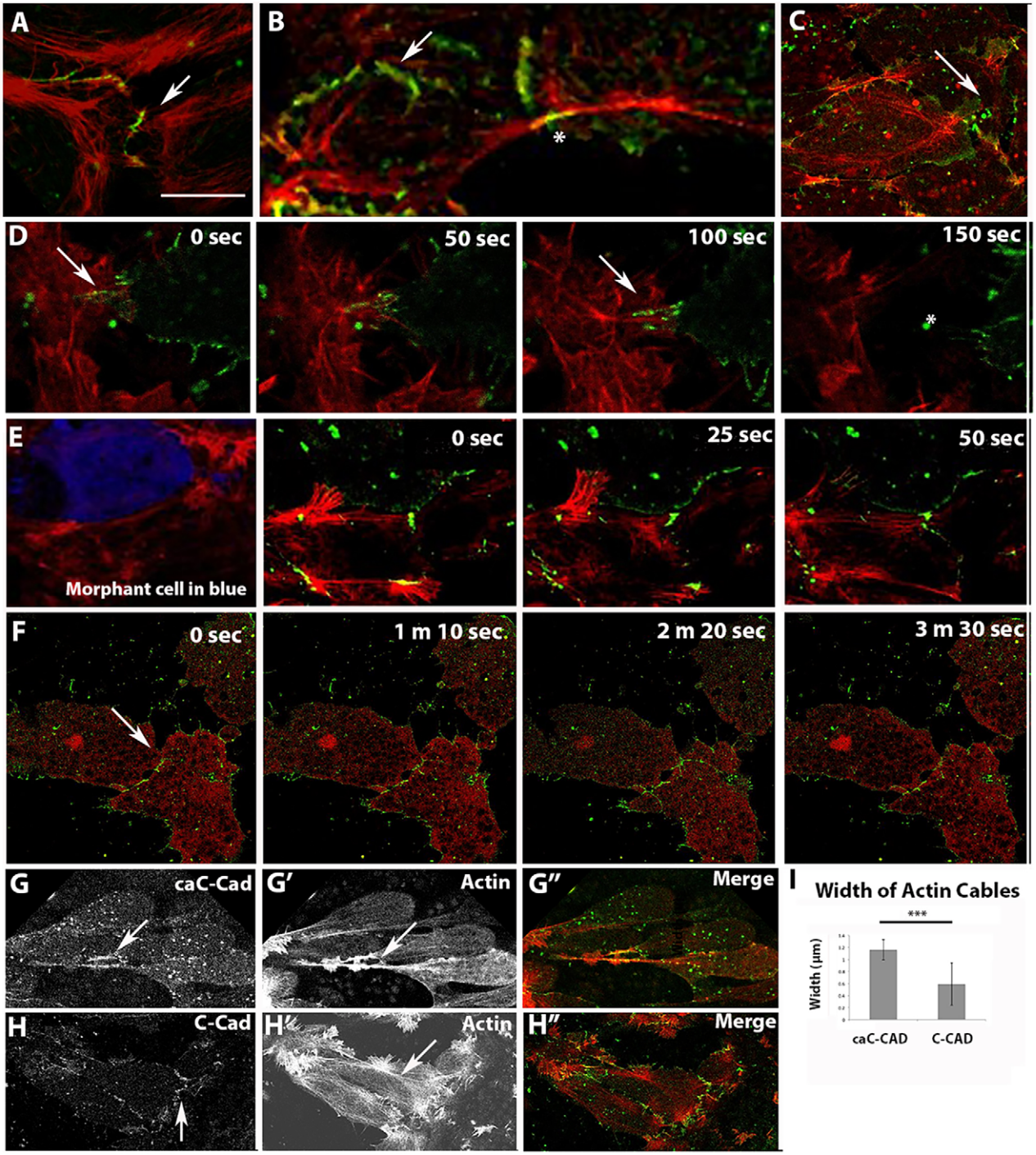

Fig. 6. C-cadherin localization on lamellipodia depends on RLC. Actin is red and C-cadherin or caC-cadherin is green. (A,B) Cadherin forms puncta (arrow) on lamellipodia (A) that resolve into long plaques (arrow), linking actin cables from neighboring cells (B, asterisk). (C) By contrast, lamellipodia on RLC morphant cells maintain a cloud of diffuse C-cadherin signal (arrow) that does not resolve into puncta. (D) Time-lapse microscopy of C-cadherin dynamics in adjacent control cells labeled singly for actin (left) or C-cadherin (right) display adhesions (arrows) that when broken, snap backwards rapidly (asterisk). (E) RLC MO-treated cells (co-injected with a blue dextran) do not make adhesions with neighboring control cells. (F) pnRLC-expressing morphant cells display little protrusive activity or adhesion remodeling (arrow). (G-I) Cells expressing caC-cadherin exhibit longer linear adhesion plaques than C-cadherin-expressing cells (arrows in G,H), which are associated with thicker actin cables (arrow in G′, quantified in I; *n*=20 widths per condition). Merged images are in G″,H″. Scale bar in A is 20 µm for all images. Error bars represent s.e.m. ***P<0.001.

and untreated cells, for example C-cadherin signal remained diffuse in extending RLC morphant lamellipodia and did not mature into clusters of cadherin plaques (Fig. 6C, Movie 11). Imaging of scattered morphant cells (Fig. 6E, blue cell) in a wild-type background showed that the depletion of RLC led to a decreased interaction between morphant and non-morphant cells (Fig. 6E, Movie 12). Wild-type cells extending lamellipodia onto a morphant neighbor failed to establish discrete C-cadherin puncta, even when the C-cadherin signal between that same cell and a neighboring wild-type cell increased. This reveals that RLC morphant cells are

Development (2016) 143, 715-727 doi:10.1242/dev.128090

defective in both generating and supporting the generation of *de novo* C-cadherin adhesions. A difference in C-cadherin dynamics is also seen between control and pnRLC-expressing morphant cells, but with a markedly different phenotype than that exhibited by RLC morphant cells (Fig. 6F). These cells in explants exhibited their characteristic reduced length-width ratio, had established contact with one another through stable C-cadherin structures and exhibited very little protrusive activity or adhesion remodeling (Movie 13).

These data support the hypothesis that MII-contractility-dependent remodeling of C-cadherin dynamics is required for CE and our observation of transcellular arrays of actomyosin networks linked by plaques of C-cadherin at the cell membranes suggests that such structures could be responsible for the transmittal of tensile force across intercalating tissue. Expression of a chimeric C-cadherin protein in which the actin-binding region from α-catenin replaces the β-catenin binding region normally present on the cytoplasmic tail of C-cadherin to allow constitutive actin binding (caC-Cad) was constructed in analogy to work previously done with E-cadherin in epithelial cells (Nagafuchi et al., 1994). Cells expressing caC-Cad-GFP localized this protein to the transcellular actomyosin arrays similar to localization of C-Cad-GFP, but generated thicker actomyosin cables in intercalating cells compared with cells expressing wild-type C-cadherin (Fig. 6G-I).

DISCUSSION

Several lines of evidence indicate that trans-cellular molecular complexes produce, transmit and spatially remodel the tensional convergence forces required for *Xenopus* CE. First is the identification of mechanically linked complexes of actomyosin and C-cadherin capable of generating and transmitting tension between cells and through intercalating tissue. These complexes appear to be under tension and mature as convergence forces rise. We propose that these complexes act as dynamic but coherent tension-bearing elements that are required for convergence to be translated into extension during CE. Second, myosin contractility supports the assembly and functioning of these complexes, generates convergence forces in explants and inhibits progress of two convergence-driven processes: blastopore closure and axial elongation in the intact embryo. These data indicate that force generated from MII contractility is required for CE. Third, C-cadherin is in position to transmit mediolateral tension and molecular perturbation at the level of C-cadherin affects transcellular arrays. These data allow us to identify a molecular mechanism that promotes cell intercalation up a force gradient. In this mechanism, lamellipodia extending medially or laterally in the tissue form nascent C-cadherin-based adhesions with neighboring cells. Analogous to focal adhesions, the nascent adhesions then mature and engage the cortical actin networks, creating a continuous linkage between actomyosin networks in neighboring cells. Contractile activity then shortens the distance between mature adhesions and the midbody of the cell to power cell intercalation. This work reveals a molecular mechanism by which a combination of dynamic MII contractility and cell adhesion are transduced into extension forces by cell intercalation, as proposed previously at the cellular level (Keller et al., 2000, 1992).

RLC molecular phenotypes show that MII contractility is essential for development of convergence forces

Depleting either RLC or MIIB blocks gastrulation; thus, both interdictions might function by destabilizing the MIIB complex (Shindo and Wallingford, 2014; Skoglund et al., 2008). To avoid this MII degradation phenotype and focus specifically on the role of T18/S19 phosphorylation in axial morphogenesis we rescued MIIB complex stability by expressing wtRLC or pnRLC proteins. These experiments revealed that one important function for RLC is to stabilize the MII complex, that this role does not depend on the phosphorylation state of the RLC and that both the wtRLC and pnRLC rescue proteins we expressed can function in the context of this complex.

In addition to protecting MII complexes from degradation, RLC proteins also regulate their contractile function through phosphorylation. Phosphorylation of RLC on Ser19, and subsequently Thr18 (T18-P; S19-P), upregulates MII complex contractility by 60- to 1000-fold in various assays and can increase assembly of MII complexes into mini-filaments, thereby regulating production of force and modulating actin-crosslinking activity (Aad et al., 2015; Sellers, 1985, 1991; Somlyo and Somlyo, 2003; Trybus, 1989; Vasquez et al., 2014; Wendt et al., 2001). Whereas both wtRLC- and pnRLC-rescued morphants exhibit stabilization of the MII complex, only wtRLC rescues blastopore closure and convergence force production, indicating a strong dependence of these force-production events on RLC phosphorylation. We exclude a neomorphic role for the pnRLC mutant protein because embryos injected with both control morpholino and pnRLC close their blastopores normally and exclude the possibility that pnRLC does not function because it rescues both MII complex levels and cell surface areas in explants. The most parsimonious explanation is that pnRLC-rescued MII complexes are compromised for force-generating MII contractility, because wtRLC- but not pnRLC-rescued morphants can both close their blastopores as whole embryos and generate normal convergence forces as explants. However, these experiments do not rule out a contribution of a second direct negative effect on the MII complex by pnRLC expression that is distinct from inhibiting contractility. Moreover, these experiments do not separate the relative roles for tension generation by MII contractility in direct generation of convergence forces as opposed to a secondary role in the establishment and maintenance of networks containing cortical actin and C-cadherin, as has been seen with E-cadherin (Liu et al., 2010). In fact, we see such molecular phenotypes in pnRLC-rescued intercalating cells, and further suggest that these elements combine into a tension-dependent transcellular molecular array responsible for the generation and propagation of convergence forces.

We interpret our findings in the following manner: (1) the morphant RLC depletion phenotype arises from a combination of MII complex destabilization and inhibition of MII complex contractility; because complex degradation occurs with a time lag of several hours (Park et al., 2011) this phenotype transitions from an initial loss of contractility towards phenocopying the loss of MIIB; (2) pnRLC-rescued depletion of RLC provides significant actin crosslinking activity but lacks contractile activity; and (3) expression of wild-type RLC fully restores force generation by restoring both crosslinking activity and MII contractility in RLC morphants. Actin phenotypes resulting from perturbing RLC phosphorylation include the reduction in the frequency and rates of actin movement in condensing proto-nodes, reduction in the number of nodes and rates of node movement in the node-and-cable actin network. These results strongly suggest that contractility operating in the context of these actomyosin structures supplies both convergence forces and the molecular machinery required for their propagation.

Spatial regulation of C-cadherin function is crucial for cell intercalation

Xenopus embryos develop arcs of convergence force across the dorsal mesodermal tissues beginning at mid-gastrulation that

Development (2016) 143, 715-727 doi:10.1242/dev.128090

function to close the blastopore, are associated with bipolar mesodermal cells and require tension to be transmitted across the multicellular tissue (Keller, 2002; Shih and Keller, 1992a,b). The mediolaterally polarized protrusions on intercalating cells are the sites at which new adhesions are made and these then become the anchor points that link to the cytoskeleton and generate traction forces on neighboring cells. This suggests that the mediolateral polarization of actomyosin structures could arise as a direct consequence of the presence of mediolaterally polarized lamellipodia (Kim and Davidson, 2011; Shih and Keller, 1992b; Skoglund et al., 2008) and both actin polarization and mediolateral cell elongation share a common dependence on the vertebrate non-canonical Wnt planar cell polarity (PCP) pathway (Goto and Keller, 2002; Kim and Davidson, 2011; Wallingford et al., 2000). Although protrusive activity does not itself generate traction forces, in its role of 'getting a new grip', it is universally associated with a subsequent traction force in traction-force microscopy of both single cells and groups of cells (Beningo et al., 2001, 2006; Harris et al., 1980; Hind et al., 2015; Lo et al., 2004, 2000). Although integrin-mediated traction forces have received most experimental attention, C-cadherin adhesion also functions in force transduction in *Xenopus* (Bjerke et al., 2014; Schwartz and DeSimone, 2008) and E-cadherin-mediated cell traction forces have also been seen during *Drosophila* border cell migration (Cai et al., 2014; Fulga and Rørth, 2002; Geisbrecht and Montell, 2002; Rauzi et al., 2010).

We hypothesize that actomyosin cables are mechanically linked across plasma membranes by C-cadherin plaques to form transcellular arrays. C-cadherin has been shown to be required for gastrulation (Lee and Gumbiner, 1995) and its adhesion activity is tightly regulated during CE, with activity decreasing without altering protein levels on the surface of intercalating cells (Brieher and Gumbiner, 1994; Zhong et al., 1999). The findings that *Xenopus* C-cadherin from two neighboring cells localizes to plaques in the context of transcellular arrays and that expression of a neomorphic C-cadherin variant with constitutive actin-binding activity causes a thickening of actin cables in intercalating cells, support our contention that C-cadherin and actomyosin are components of a molecular machine capable of producing and transmitting tension during gastrulation. Moreover, this suggests that cellular regulation of actin-binding activity to the intercellular tail of the normal C-cadherin in intercalating cells is an important control point for CE. Such locally mediated cellular regulation has been shown to support assembly of distinct actomyosin structures in different regions of individual cells (Scott et al., 2006) and we have previously shown that perturbing the

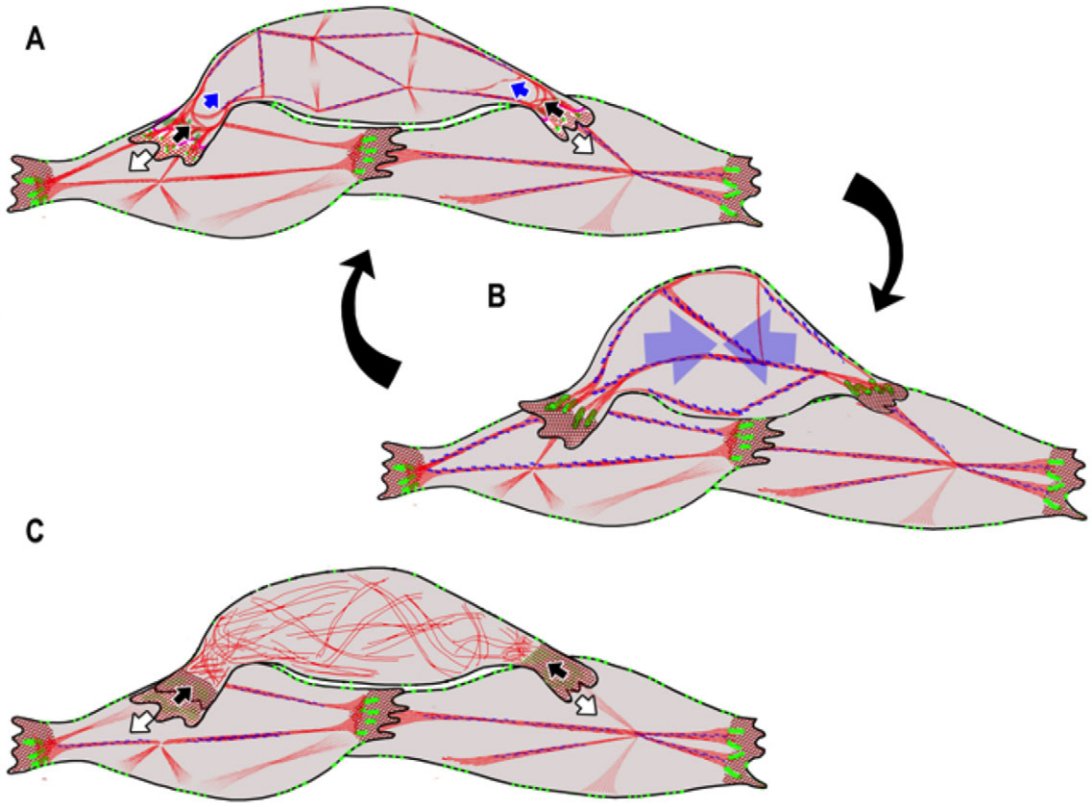

Fig. 7. Summary of the roles of myosin II contractility, actin cytoskeleton and C-cadherin dynamics in generating the convergence force driving cell intercalation during CE. (A) Deep dorsal mesodermal cells extend large filo-lamelliform protrusions in the medial and lateral directions (white arrows), a protrusive activity characterized by a diffuse actin network (red cross-hatching). These attach to neighboring cells by *de novo* formation of small, nascent C-cadherin puncta (bright green). As the actin network undergoes retrograde flow toward the cell body, it coalesces into a series of intersecting arcs, called 'proto-nodes' (black arrows), which mature into a characteristic 'node-and-cable' actin cytoskeleton spanning the cell body (red cables and intersections). (B) The node-and-cable system undergoes a mediolaterally oriented, actomyosin-mediated contraction (blue arrows, A,B), thereby generating tension that shortens the cell, exerts traction on the neighboring cells, drives mediolateral cell intercalation, and generates a tissue-level, tensile convergence force. This mechanism consists of two interlinked and iterated molecular cycles, first an adhesion cycle (A) consisting of nascent, C-cadherin plaques arising on polarized lamellipodia, which mature into larger, linear actin containing plaques that link the cytoskeletons of individual cells together in a tissue-level system in a contraction-dependent manner, and second, a cytoskeletal cycle (B) consisting of a mediolaterally oriented tension-generating actomyosin contraction. Both cycles are dependent on a contractile myosin II complex (blue arrows in A,B), as the maturation of cadherin puncta into mature adhesion plaques, the maturation of the protrusive cytoskeleton into protonodes and those into the polarized node-and-cable system; all fail in RLC morphants (C).

Development (2016) 143, 715-727 doi:10.1242/dev.128090

cortical actin network during CE by targeting myosin IIB heavy chain also reduces C-cadherin-based adhesion activity without altering receptor levels on the cell surface (Skoglund et al., 2008). *Xenopus* C-cadherin can either be diffusely distributed or localized to puncta on the cell membrane and we find that this localization within the membrane, formation of puncta on the cell body, as well as the formation of new puncta on lamellipodia, are dependent on MII contractility. This is consistent with the idea that local tensional state of cytoskeleton regulates C-cadherin dynamics, as has been described in cell culture (Liu et al., 2010).

Summary of the role of myosin II contractility and dynamic C-cadherin distribution in CE

To summarize the molecular machinery proposed to drive CE, initially unpolarized deep mesodermal cells become polarized and form large, mediolaterally oriented lamelliform protrusions that participate in an iterated cycle of motility, adhesion, and contraction. As these lamellipodia preferentially extend in the mediolateral axis, they elongate the cell, extend its 'reach' onto neighboring cell bodies and establish adhesions to these neighboring cells in the form of nascent C-cadherin puncta between their cell bodies and the lamellipodia (Fig. 7A). As the actin filament cytoskeleton of the lamella undergoes retrograde flow towards the cell body, it forms interlocking arcs or 'proto-nodes', which subsequently mature to form the definitive 'node-and-cable' cytoskeleton of the cell body. The proto-node and node-and-cable undergoes cycles of contraction and relaxation linked to these mediolaterally biased anchor points, and generation of mediolaterally polarized, repetitive traction forces, which are invariably associated with these types of protrusions. The nascent C-cadherin puncta mature into larger, linear C-cadherin adhesion plaques, which become linked to the actin cytoskeleton and connect the contractile activity in individual cells in a tensile array spanning the mediolateral aspect of the tissue. The formation of the characteristic node-and-cable actin cytoskeleton, the maturation of the C-cadherin adhesions and the emergence of mediolateral polarity, are all dependent on RLC (Fig. 7C). The C-cadherin adhesions link the intracellular contractile node-and-cable cytoskeletal systems in each cell into a large, transcellular tensile array. Because these adhesions are both modulated as the cells intercalate and eventually turn over, the exact path of tensile forces through the tissue varies, but it is always present and intact.

MATERIALS AND METHODS

Embryos and manipulations

Xenopus laevis embryos and explants were generated (Skoglund et al., 2008), and MO and mRNA injections were made into both cells at the 2-cell stage or dorsally targeted into single blastomeres at 32-cell stage (Lee and Gumbiner, 1995), as described. Final concentrations of MO were 1-15 µM, mRNA was 1-2 ng per embryo equivalent, and Ruby-labeled dextran was at 1-2 µg per embryo equivalent in the injected cell. The tractor-pull experiments consist of measuring the convergence forces generated by sandwich marginal zone explants by monitoring the deflection of a mechanically coupled fiber optic probe with a known spring constant. For further details, see supplementary Materials and Methods.

Morpholinos and expression plasmids

A morpholino directed against RLC from Myl-12B (5-GGTCTTTGCTC-TTTTGCTGGACATC-3) was produced (Gene Tools). wtRLC and pnRLC constructs were made with a MO-insensitive N-terminal end from Myl-12B sequences, adding a C-terminal mCherry tag. Moesin-GFP was as described (Skoglund et al., 2008). LifeAct-mCherry was made in $pCS2^{+}$, whereas C-cadherin-GFP, C-cadherin-tomato and caC-cadherin-GFP were made in pCS105. In caC-Cad, the β-catenin-binding domain of C-cadherin was replaced with the actin-binding domain of α-catenin. Capped RNA was from the mMessage mMachine Kit (Ambion). For further details, see supplementary Materials and Methods.

Whole-mount immunohistochemistry and western blotting

Embryo lysates were generated (Stukenberg et al., 1997) and resolved by SDS-PAGE (Skoglund and Keller, 2007) as described, except 4-20% gradient gels and the Odyssey-LiCor imaging system were used.

Explants for whole-mount immunohistochemistry were fixed in two stages modified from Becker and Gard, 2005; Luther and Bloch, 1989. Further details are available in supplementary Materials and Methods. Antibodies were anti-RLC (Santa Cruz Biotechnology, sc15370; 1:200), anti-RLC Ser19P (Cell Signaling, 3675; 1:500), anti-C-cadherin (DSHB, 6B6; 1:250), and anti-MHC-IIB (Sigma, M7939; 1:2000).

Imaging and analysis

Low-magnification images were taken using an Olympus SZX16 stereoscope with a DP72 camera. Blastopore closure images were taken on an Olympus IX70 with a Hamamatsu C4742 camera and collected using Metamorph software at a rate of 1 frame/3 min for 12 h. Zeiss 510Meta and 780 confocal microscopes were used for imaging of live and fixed explants, using 25× or 63× objectives and line averaging. Time lapses had a 5-15 s framing rate and *Z*-stacks had 1 µm or 0.1 µm steps. Foci tracking and kymographs were done using the 'Manual Tracker' or 'Multiple Kymograph' plug-ins for ImageJ (NIH) software and the angle and length of kymograph lines measured in ImageJ.

Acknowledgements

The 6B6 antibody was procured from the DSHB and concentrated in the Wiley lab. We thank Dr Dorothy Schafer and Dr Ammasi Periasamy for comments, advice and discussions.

Competing interests

The authors declare no competing or financial interests.

Author contributions

K.P., R.K. and P.S. developed the approach. K.P., P.S. and D.R.S. performed experiments. C.C. developed the C-cadherin constructs. K.P. wrote the paper, and R.K. and P.S. edited the paper.

Funding

This work was supported by the National Institutes of Health [RR021202, ODO16446, HD069297 to C.C.; MERIT Award R37 HD025594 and related supplement HD025594-S1ARRA to R.K. and GM099108 to P.S.] We thank the Institutes of Child Health and General Medicine at the NIH. K.P. was partially funded by an NIH training grant [GM008136]. Deposited in PMC for release after 12 months.

Supplementary information

Supplementary information available online at
http://dev.biologists.org/lookup/suppl/doi:10.1242/dev.128090/-/DC1

References

Aad, G., Abbott, B., Abdallah, J., Abdel Khalek, S., Abdinov, O., Aben, R., Abi, B., Abolins, M., AbouZeid, O. S., Abramowicz, H. et al. (2015). Search for Higgs and Z Boson Decays to J/psigamma and Upsilon(nS)gamma with the ATLAS Detector. *Phys. Rev. Lett.* **114**, 121801.

Becker, B. and Gard, D. L. (2005). Visualization of the Cytoskeleton in *Xenopus* Oocytes and Eggs by Confocal Immunofluorescence Microscopy. In *Xenopus Protocols: Cell Biology and Signal Transduction*. *Meth. Mol. Biol.* 322, 69-86.

Beningo, K. A., Dembo, M., Kaverina, I., Small, J. V. and Wang, Y.-l. (2001). Nascent focal adhesions are responsible for the generation of strong propulsive forces in migrating fibroblasts. *J. Cell Biol.* **153**, 881-888.

Beningo, K. A., Hamao, K., Dembo, M., Wang, Y.-l. and Hosoya, H. (2006). Traction forces of fibroblasts are regulated by the Rho-dependent kinase but not by the myosin light chain kinase. *Arch. Biochem. Biophys.* **456**, 224-231.

Bjerke, M. A., Dzamba, B. J., Wang, C. and DeSimone, D. W. (2014). FAK is required for tension-dependent organization of collective cell movements in Xenopus mesendoderm. *Dev. Biol.* **394**, 340-356.

Brieher, W. M. and Gumbiner, B. M. (1994). Regulation of C-cadherin function during activin induced morphogenesis of Xenopus animal caps. *J. Cell Biol.* **126**, 519-527.
Buisson, N., Sirour, C., Moreau, N., Denker, E., Le Bouffant, R., Goullancourt, A., Darribere, T. and Bello, V. (2014). An adhesome comprising laminin, dystroglycan and myosin IIA is required during notochord development in Xenopus laevis. *Development* **141**, 4569-4579.
Cai, D., Chen, S.-C., Prasad, M., He, L., Wang, X., Choesmel-Cadamuro, V., Sawyer, J. K., Danuser, G. and Montell, D. J. (2014). Mechanical feedback through E-cadherin promotes direction sensing during collective cell migration. *Cell* **157**, 1146-1159.
Davidson, L. A., Keller, R. and DeSimone, D. W. (2004). Assembly and remodeling of the fibrillar fibronectin extracellular matrix during gastrulation and neurulation in *Xenopus laevis*. *Dev. Dyn.* **231**, 888-895.
Davidson, L. A., Marsden, M., Keller, R. and DeSimone, D. W. (2006). Integrin alpha5beta1 and fibronectin regulate polarized cell protrusions required for Xenopus convergence and extension. *Curr. Biol.* **16**, 833-844.
Fernandez-Gonzalez, R. and Zallen, J. A. (2011). Oscillatory behaviors and hierarchical assembly of contractile structures in intercalating cells. *Phys. Biol.* **8**, 045005.
Fulga, T. A. and Rørth, P. (2002). Invasive cell migration is initiated by guided growth of long cellular extensions. *Nat. Cell Biol.* **4**, 715-719.
Geisbrecht, E. R. and Montell, D. J. (2002). Myosin VI is required for E-cadherin-mediated border cell migration. *Nat. Cell Biol.* **4**, 616-620.
Glickman, N. S., Kimmel, C. B., Jones, M. A. and Adams, R. J. (2003). Shaping the zebrafish notochord. *Development* **130**, 873-887.
Goto, T. and Keller, R. (2002). The planar cell polarity gene strabismus regulates convergence and extension and neural fold closure in Xenopus. *Dev. Biol.* **247**, 165-181.
Goto, T., Davidson, L., Asashima, M. and Keller, R. (2005). Planar cell polarity genes regulate polarized extracellular matrix deposition during frog gastrulation. *Curr. Biol.* **15**, 787-793.
Harris, A. K., Wild, P. and Stopak, D. (1980). Silicone rubber substrata: a new wrinkle in the study of cell locomotion. *Science* **208**, 177-179.
He, L., Wang, X., Tang, H. L. and Montell, D. J. (2010). Tissue elongation requires oscillating contractions of a basal actomyosin network. *Nat. Cell Biol.* **12**, 1133-1142.
He, B., Doubrovinski, K., Polyakov, O. and Wieschaus, E. (2014). Apical constriction drives tissue-scale hydrodynamic flow to mediate cell elongation. *Nature* **508**, 392-396.
Hind, L. E., Dembo, M. and Hammer, D. A. (2015). Macrophage motility is driven by frontal-towing with a force magnitude dependent on substrate stiffness. *Integr. Biol.* **7**, 447-453.
Keller, R. (2002). Shaping the vertebrate body plan by polarized embryonic cell movements. *Science* **298**, 1950-1954.
Keller, R. (2006). Mechanisms of elongation in embryogenesis. *Development* **133**, 2291-2302.
Keller, R. and Danilchik, M. (1988). Regional expression, pattern and timing of convergence and extension during gastrulation of *Xenopus laevis*. *Development* **103**, 193-209.
Keller, R., Shih, J. and Domingo, C. (1992). The patterning and functioning of protrusive activity during convergence and extension of the Xenopus organiser. *Development* Suppl., 81-91.
Keller, R., Davidson, L., Edlund, A., Elul, T., Ezin, M., Shook, D. and Skoglund, P. (2000). Mechanisms of convergence and extension by cell intercalation. *Philos. Trans. R. Soc. B Biol. Sci.* **355**, 897-922.
Kim, H. Y. and Davidson, L. A. (2011). Punctuated actin contractions during convergent extension and their permissive regulation by the non-canonical Wnt-signaling pathway. *J. Cell Sci.* **124**, 635-646.
Lee, C.-H. and Gumbiner, B. M. (1995). Disruption of gastrulation movements in Xenopus by a dominant-negative mutant for C-cadherin. *Dev. Biol.* **171**, 363-373.
Liu, Z., Tan, J., Cohen, D., Yang, M., Sniadeki, N., Ruiz, S., Nelson, C. and Chen, C. (2010). Mechanical tugging force regulates the size of cell-cell junctions. *Proc. Natl. Acad. Sci. USA* **107**, 9944-9949.
Lo, C.-M., Wang, H.-B., Dembo, M. and Wang, Y.-l. (2000). Cell movement is guided by the rigidity of the substrate. *Biophys. J.* **79**, 144-152.
Lo, C.-M., Buxton, D. B., Chua, G. C. H., Dembo, M., Adelstein, R. S. and Wang, Y.-L. (2004). Nonmuscle myosin IIb is involved in the guidance of fibroblast migration. *Mol. Biol. Cell* **15**, 982-989.
Luther, P. W. B. and Bloch, R. J. (1989). Formaldehyde-amine fixatives for immunocytochemistry of cultured Xenopus myocytes. *J. Histochem. Cytochem.* **37**, 75-82.
Martin, A. C., Kaschube, M. and Wieschaus, E. F. (2009). Pulsed contractions of an actin–myosin network drive apical constriction. *Nature* **457**, 495-499.
Moore, S. W. (1994). A fiber optic system for measuring dynamic mechanical properties of embryonic tissues. *IEEE Trans. Biomed. Eng.* **41**, 45-50.
Moore, S. W., Keller, R. E. and Koehl, M. A. (1995). The dorsal involuting marginal zone stiffens anisotropically during its convergent extension in the gastrula of *Xenopus laevis*. *Development* **121**, 3131-3140.
Munro, E., Nance, J. and Priess, J. R. (2004). Cortical flows powered by asymmetrical contraction transport PAR proteins to establish and maintain anterior-posterior polarity in the early *C. elegans* embryo. *Dev. Cell* **7**, 413-424.
Nagafuchi, A., Ishihara, S. and Tsukita, S. (1994). The roles of catenins in the Cadherin-mediated cell adhesion: functional analysis of E-Cadherin-alpha catenin fusion molecules. *J. Cell Biol.* **127**, 235-245.
Park, I., Han, C., Jin, S., Lee, B., Choi, H., Kwon, J. T., Kim, D., Kim, J., Lifirsu, E., Park, W. J. et al. (2011). Myosin regulatory light chains are required to maintain the stability of myosin II and cellular integrity. *Biochem. J.* **434**, 171-180.
Poznanski, A. and Keller, R. (1997). The role of planar and early vertical signaling in patterning the expression of Hoxb-1 in Xenopus. *Dev. Biol.* **184**, 351-366.
Rauzi, M., Lenne, P.-F. and Lecuit, T. (2010). Planar polarized actomyosin contractile flows control epithelial junction remodelling. *Nature* **468**, 1110-1114.
Rolo, A., Skoglund, P. and Keller, R. (2009). Morphogenetic movements driving neural tube closure in Xenopus require myosin IIB. *Dev. Biol.* **327**, 327-338.
Rozario, T., Dzamba, B., Weber, G. F., Davidson, L. A. and DeSimone, D. W. (2009). The physical state of fibronectin matrix differentially regulates morphogenetic movements in vivo. *Dev. Biol.* **327**, 386-398.
Sater, A. K., Steinhardt, R. A. and Keller, R. (1993). Induction of neuronal differentiation by planar signals in Xenopus embryos. *Dev. Dyn.* **197**, 268-280.
Sawyer, J. K., Harris, N. J., Slep, K. C., Gaul, U. and Peifer, M. (2009). The Drosophila afadin homologue Canoe regulates linkage of the actin cytoskeleton to adherens junctions during apical constriction. *J. Cell Biol.* **186**, 57-73.
Schwartz, M. A. and DeSimone, D. W. (2008). Cell adhesion receptors in mechanotransduction. *Curr. Opin. Cell Biol.* **20**, 551-556.
Scott, J. S., Shewan, A. M., den Elzen, N., Loureiro, J. J., Gertler, F. R. and Yap, A. S. (2006). Ena/VASP proteins can regulate distinct modes of actin organization at Cadherin-adhesive contacts. *Mol. Biol. Cell* **17**, 1085-1095.
Sellers, J. R. (1985). Mechanism of the phosphorylation-dependent regulation of smooth muscle heavy meromyosin. *J. Biol. Chem.* **260**, 15815-15819.
Sellers, J. R. (1991). Regulation of cytoplasmic and smooth muscle myosin. *Curr. Opin. Cell Biol.* **3**, 98-104.
Shih, J. and Keller, R. (1992a). Patterns of cell motility in the organizer and dorsal mesoderm of Xenopus laevis. *Development* **116**, 915-930.
Shih, J. and Keller, R. (1992b). Cell motility driving mediolateral intercalation in explants of Xenopus laevis. *Development* **116**, 901-914.
Shindo, A. and Wallingford, J. B. (2014). PCP and septins compartmentalize cortical actomyosin to direct collective cell movement. *Science* **343**, 649-652.
Skoglund, P. and Keller, R. (2007). Xenopus fibrillin regulates directed convergence and extension. *Dev. Biol.* **301**, 404-416.
Skoglund, P., Dzamba, B., Coffman, C. R., Harris, W. A. and Keller, R. (2006). Xenopus fibrillin is expressed in the organizer and is the earliest component of matrix at the developing notochord-somite boundary. *Dev. Dyn.* **235**, 1974-1983.
Skoglund, P., Rolo, A., Chen, X., Gumbiner, B. M. and Keller, R. (2008). Convergence and extension at gastrulation require a myosin IIB-dependent cortical actin network. *Development* **135**, 2435-2444.
Solnica-Krezel, L. and Sepich, D. S. (2012). Gastrulation: making and shaping germ layers. *Annu. Rev. Cell Dev. Biol.* **28**, 687-717.
Somlyo, A. P. and Somlyo, A. V. (2003). Ca2+ sensitivity of smooth muscle and nonmuscle myosin II: modulated by G proteins, kinases, and myosin phosphatase. *Physiol. Rev.* **83**, 1325-1358.
Stukenberg, P. T., Lustig, K. D., McGarry, T. J., King, R. W., Kuang, J. and Kirschner, M. W. (1997). Systematic identification of mitotic phosphoproteins. *Curr. Biol.* **7**, 338-348.
Trybus, K. M. (1989). Filamentous smooth muscle myosin is regulated by phosphorylation. *J. Cell Biol.* **109**, 2887-2894.
Vasquez, C. G., Tworoger, M. and Martin, A. C. (2014). Dynamic myosin phosphorylation regulates contractile pulses and tissue integrity during epithelial morphogenesis. *J. Cell Biol.* **206**, 435-450.
Vicente-Manzanares, M., Ma, X., Adelstein, R. S. and Horwitz, A. R. (2009). Non-muscle myosin II takes centre stage in cell adhesion and migration. *Nat. Rev. Mol. Cell Biol.* **10**, 778-790.
Wallingford, J. B., Rowning, B. A., Vogeli, K. M., Rothbächer, U., Fraser, S. E. and Harland, R. M. (2000). Dishevelled controls cell polarity during Xenopus gastrulation. *Nature* **405**, 81-85.
Wang, A., Ma, X., Conti, M. A. and Adelstein, R. S. (2011). Distinct and redundant roles of the non-muscle myosin II isoforms and functional domains. *Biochem. Soc. Trans.* **39**, 1131-1135.
Wendt, T., Taylor, D., Trybus, K. M. and Taylor, K. (2001). Three-dimensional image reconstruction of dephosphorylated smooth muscle heavy meromyosin reveals asymmetry in the interaction between myosin heads and placement of subfragment 2. *Proc. Natl. Acad. Sci. USA* **98**, 4361-4366.
Williams, M., Yen, W., Lu, X. and Sutherland, A. (2014). Distinct apical and basolateral mechanisms drive planar cell polarity-dependent convergent extension of the mouse neural plate. *Dev. Cell* **29**, 34-46.
Wilson, P. and Keller, R. (1991). Cell rearrangement during gastrulation of Xenopus: direct observation of cultured explants. *Development* **112**, 289-300.

Development (2016) 143, 715-727 doi:10.1242/dev.128090

Yen, W. W., Williams, M., Periasamy, A., Conaway, M., Burdsal, C., Keller, R., Lu, X. and Sutherland, A. (2009). PTK7 is essential for polarized cell motility and convergent extension during mouse gastrulation. *Development* **136**, 2039-2048.

Zhong, Y., Brieher, W. M. and Gumbiner, B. M. (1999). Analysis of C-cadherin regulation during tissue morphogenesis with an activating antibody. *J. Cell Biol.* **144**, 351-359.

Zhou, J., Kim, H. Y. and Davidson, L. A. (2009). Actomyosin stiffens the vertebrate embryo during crucial stages of elongation and neural tube closure. *Development* **136**, 677-688.

Zhou, J., Pal, S., Maiti, S. and Davidson, L. A. (2015). Force production and mechanical accommodation during convergent extension. *Development* **142**, 692-701.

Supplementary Materials and Methods

Whole mount fixation

Explants or embryos were fixed in two stages, first in a 0.45% Formaldehyde, 75mM cyclohexylamine solution, pH 6.5, for 45 min at room temperature, then in a MEMFA solution (3.7% Formaldehyde, 0.25% Glutaraldehyde, 5% DMSO solution, pH 7.8) for 1 hour. Blocking solution was 10% FBS, 1% BSA, 5% DMSO, and 0.1% TritonX-100.

Morpholinos and Expression Constructs

A morpholino and control morpholino (varied at five nucleotides) oligonucleotide (MO and COMO) directed against RLC from Myl-12B (5-GGTCTTTGCTCTTTTGCTGGACATC-3); (COMO-5-GGTGTTAGCTCATTAGCTGGAGATC-3) were produced (Gene Tools, Philomath, OR). This RLC morpholino varies at three locations from another RLC morpholino derived from Myl-9 (Shindo and Wallingford, 2014), however both experiments use the same set of antibodies to assay RLC depletion. Both wtRLC-GFP and pnRLC-GFP were generated from Myl-12 sequences with the following modifications near the translation start site to make them insensitive to morpholino: ATG TCC AGC AAA AGA GCA AAG ACC AAG was changed to ATG agC tcC AAg cGg GCg AAa ACg AAG, however these changes did not affect the coding sequence of MSSKRAKTK. A linker sequence consisting of CGA ATT CTG CAG TCG ACG GTA CCG CGG GCC CGG GAT CCA CCG GTC GCC ACC was inserted between RLC sequences and mCherry sequences in both constructs. pnRLC was also modified internally by changing the coding sequence of Myl12B, changing ACA TCC to GCC GCC; this had the effect of changing the amino acid sequence of the resulting translation product from 16-RATSNV-21 to 16-RAAASV-21. C-Cad-GFP was generated by PCR of C-Cad sequence followed by its digestion with EcoRI/KpnI and ligation with KpnI/NotI fragment of pEGFP-N2 plasmid (from Clontech). The ligation product was inserted into the EcoRI/NotI digested pCS105 vector. C-Cad-tdTomato was constructed by replacing the GFP sequence of C-Cad-GFP with tdTomato sequence via ligation of the PCR

product from pRSET-B-tdTomato plasmid (kindly provided by Dr. Roger Tsien). caC-Cad-GFP was generated in two steps. caC-Cad was first constructed by ligation of the EcoRI/BamHI N-terminal fragment of C-Cad (with its beta-catenin binding domain removed) with the BamHI/XbaI fragment of alpha-catenin (also without its beta-catenin binding domain). The ligation product was inserted into the EcoRI/XbaI sites of pCS105. caC-Cad-GFP was subsequently generated by inserting the GFP sequence in frame at the C-terminal end of caC-Cad, using a PCR-based strategy.

Tractor Pull

Embryos were tipped and marked after fertilization to indicate the future dorsal side (Sive et al., 2000). Experimental embryos were injected in both blastomeres at 2-cell stage or into the dorsal 2 blastomeres at 4 cell stage, to a final concentration of 10 μM with RLC MO, RLC MO + pnRLC mRNA or RLC MO + wt RLC mRNA.

Force measurements were performed on paired ("giant sandwich") explants cut at stages between 8.5 to 10. Explants were made in DFA (Danilchiks for Amy) solution (Sater et al., 1993), as were all further manipulations and measurements. Force measurements were obtained using the "Tractor Pull" device shown in Fig 3A, consisting of FN coated sled and anchor strips (red in the figure; anchor attached to substrate via silicon grease (pink)) to which marginal zone explants (grey) are attached. As the explants converge mediolaterally (left-right) a cleat (yellow) attached to the sled pulls against a calibrated fiber-optic probe. Glass beads (blue dots) under the sled reduce friction. Marginal zone explants were cut from control or experimental embryos, linearized by cutting through ventral midline and the ventral ends of the explants adhered to the top ot bottom of fibronection coated sled and anchor strips, such that the mediolateral axis of both explants comprising the sandwich ran between the sled and anchor strips. Because RLC MO injected explants adhere poorly to the strips (Skoglund et al., 2008), we used dorsally injected embryos to allow ventral tisue to adhere. We used 250 μm glass beads throughout these experiments, as we found that they reduced friction between the sled and the underlying coverslip to a greater extent than the 100 μm beads used initially. After healing onto the strips, sled-explant-anchor assemblies were placed in close proximity to the force measuring probe and developed

tension on the probe as they converged along their mediolateral axis. During force measurment, explants were imaged at low resolution (6 to 7 microns per pixel) and the probe position was imaged at higher resolution (1.3 microns per pixel), and time-lapse recordings of both were made at a rate of 1 frame per 3 minutes. Probe displacement was analyzed using Image J, and force was determined by multiplying displacement by the spring constant of the probe (12.1 μN/mm).

Movie 1. Four clips from a 63x confocal time lapse movie that play at 8 frames per second with a 5 second interval. Dorsal Marginal Zone (DMZ) explants made from embryos exhibiting mosaic expression of C-Cad:GFP and Life-Act:mCherry exhibit cells in the four characteristic phases of MIB behavior. Phase 1 cells (first panel on the left) maintain the cortical actin network with an isodiametric lamellar appearance. These cells exhibit small lamellipodial protrusions that are unpolarized with respect to the embryonic axis, and C-Cadherin (C-Cad) outlines the periphery of the cell with little dynamic rearrangement. During Phase 2 the actin protrusions become fewer but larger (second panel; note the elongated lamellipodia on the bottom left of the cell shown in this movie), breaking the symmetry of Phase 1 cells. C-Cad reorganizes to accommodate the new protrusion profile, forming distinct puncta (bottom left) or elongated adhesions (top left) associated with actin. Phase 3 cells (third panel) are elongated in the mediolateral axis and the cortical actin begins to form proto-node structures associated with large polarized protrusions. C-Cad signal is more abundant and becomes distinctly polarized, exhibiting two patterns: large clusters of adhesions associated within lamellipodia (bottom left) and lower density puncta on the anterior-posterior faces (top right) of the cell. In Phase 4 (fourth panel), the actin cytoskeleton adopts the node and cable structure of thick bundles of actin cables that contract and relax at foci, often in concert with neighboring cells. These neighboring actomyosin arrays are attached with strong linear C-Cad signal that likewise oscillates in concert with local contractions.

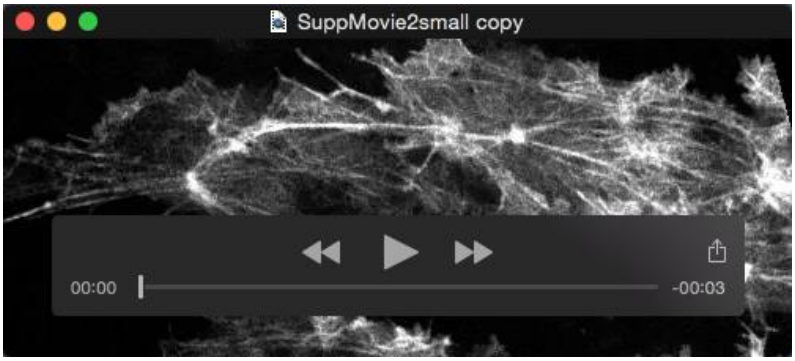

Movie 2. Confocal timelapse taken at 63x in a St. 13 DMZ explant with at 15 second interval and playing at 9 frames per second. This explant was made from an embryo mosaically expressing moe-GFP to visualize actin. Mature node and cable actomyosin networks that have clearly defined foci or "nodes" connected by thick bundles or "cables' are seen in adjacent cells. The nodes undergo long tracks of oscillating movement during cycles of local cell contraction and relaxation, and are observed to move in concert across neighboring cells. Because convergence forces are biased in the mediolateral direction, and these larger cables also run predominantly mediolaterally, the cables are correctly positioned to be elements in a chain capable of carrying tension across intercalating tissue.

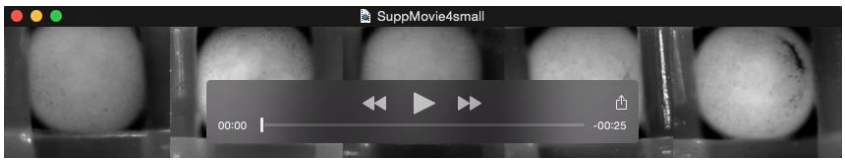

Movie 3. Blastopore closure is filmed with a 3 minute framing rate on an inverted Olympus stereoscope and plays at 12 frames per second. Blastopore closure rate is indicative of Convergence and Extension (CE) progression. Normal blastopore closure begins with the appearance of a line of concentrated pigment, resulting from apical constriction of bottle cells on the dorsal side of the embryo at stage 10 (beginning of gastrulation; start of movie). Apical constriction spreads progressively laterally and ventrally to create the blastopore through which marginal zone tissue involutes and becomes definitive mesoderm in normal embryos (first embryo on left). An RLC morphant embryo (second embryo) exhibits a decreased rate of closure, and fails to fully close its blastopore, a phenotype that is rescued by wtRLC expression (third embryo), but not pnRLC expression (fourth embryo). When pnRLC is expressed in a COMO injected embryo background, there is no effect on BC (fifth embryo).

Movie 4. Movies 4-7 are all 63x confocal time lapses of mosaic Moesin:GFP expression in St. 12 explant, with a 5 second framing rate and playing at 8 frames per second. Cells in a control DMZ display typical Phase 3 cortical actin structures and behaviors. Proto-nodes condense and relax and cells actively send out protrusions on neighbors. Here we compare actin behaviors between Movies 4-7, with this as the control movie.

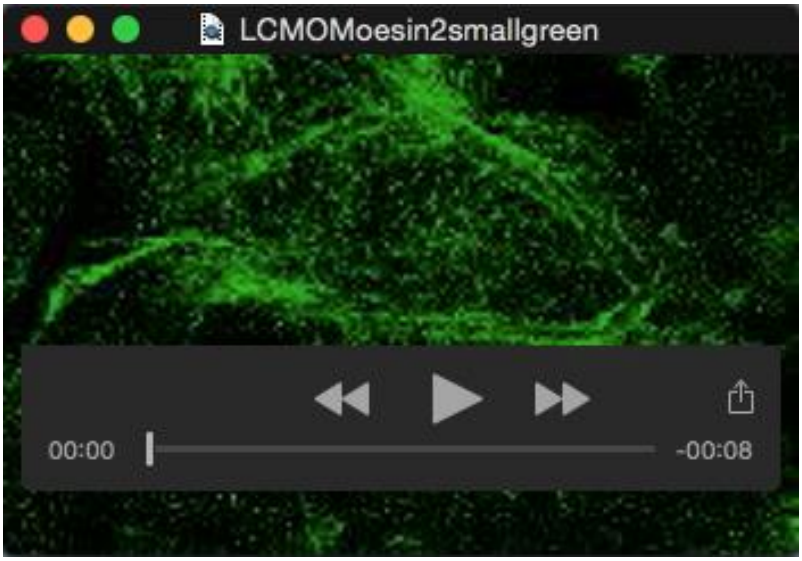

Movie 5. Similar to Movie 4, but examining the cortical actin network in RLC morphant cells. Actin movement in regions other than protrusions is generally less rapid than in control cells (compare to Movie 4). Note that retrograde flow in the lamellipodia region is continuous, but the turnover of retraction and new protrusion formation is greatly reduced. The network across the cortex is less defined; there are few thick actin cables, remaining in a fine meshwork that is difficult to resolve. The cables that do appear are short lived, lasting only one round of contraction.

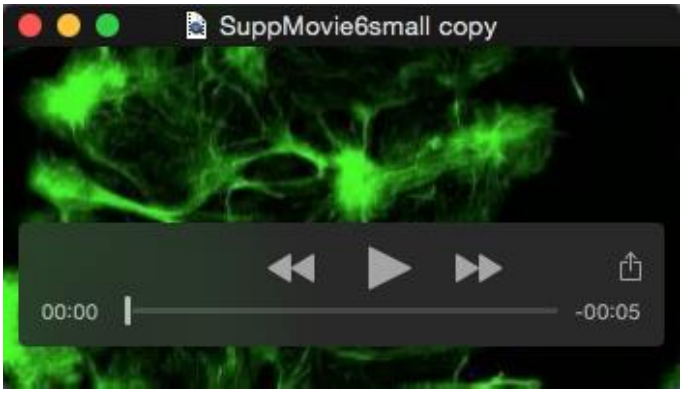

Movie 6. Similar to Movie 4, but examining the cortical actin network in RLC morphant cells that are also expressing wtRLC. Actin movement is generally more rapid than in RLC morphant cells (compare to Movie 5), and similar to control cells (compare to Movie 4). In addition to rates of actin movement, expression of wtRLC also restores the presence of nodes. Cables are also rescued, and appear to link cells together in primarily the mediolateral direction, however the rate of node condensation is not fully rescued.

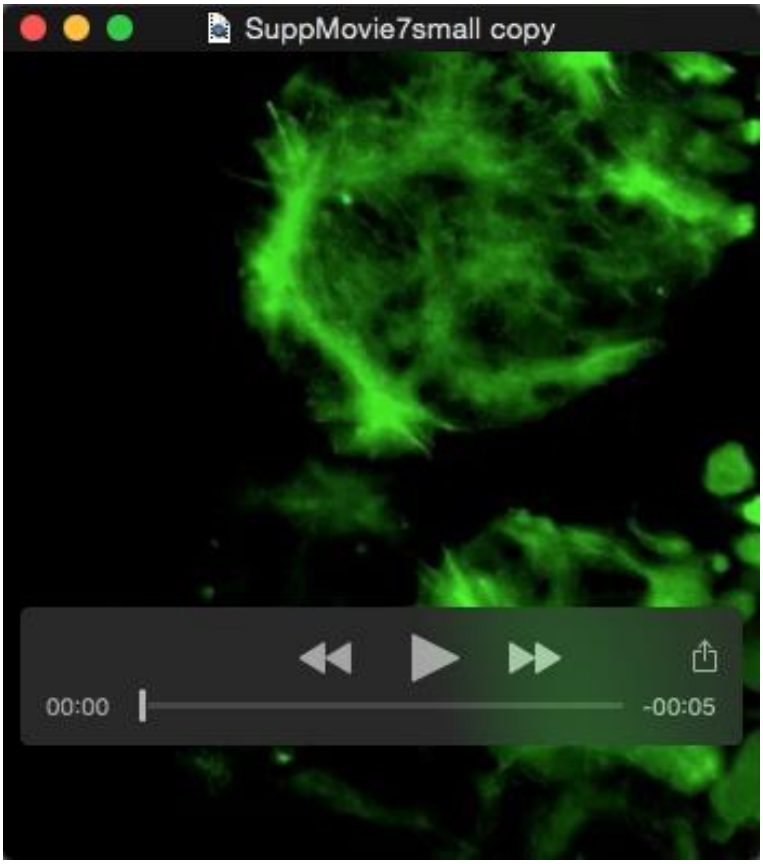

Movie 7. Similar to Movie 4, but examining the cortical actin network in RLC morphant cells that are also expressing pnRLC. Actin movement is generally retarded as compared to control or morphant plus wtRLC expressing cells (see Movies 4, 6), but similar to RLC morphant cells (see Movie 5). There is a fine meshwork of thinner actin bundles across the cortex of the cells, and few foci. They do not exhibit node oscillations and they appear predominantly at the cell periphery rather than throughout the cell cortex. In these cells, the rate of actin movement, cell contraction events, and protrusive activity are severely retarded compared to controls.

Movie 8. Confocal time lapse of cells in a St. 12 explant taken at 180x with a 5 second interval and playing at 8 frames per second. This explant was made from an embryo expressing both C-Cadherin:GFP and Life-Act:mCherry. Here we image C-Cad puncta (green) and actin (red) on a mediolaterally-biased lamellipodia from a cell in Phase 3 of MIB, providing support for our hypothesis that cell-on-cell traction is driven by lamellipodial protrusions during CE. The actin exhibits characteristic rearward flow and actin polymerization at the distal end, and the relationship between C-Cad and actin dynamics suggests these structures collaborate to generate traction force. Puncta of C-Cad on the membrane are clustered densely at the lamellipodial protrusion and can be seen to move within the membrane, reinforcing contacts involving thicker actin bundles between neighboring cells. As the protrusion locally retracts, the C-Cad signal is diluted, suggesting rapid dynamic regulation of actin and C-Cad during cell-cell traction.

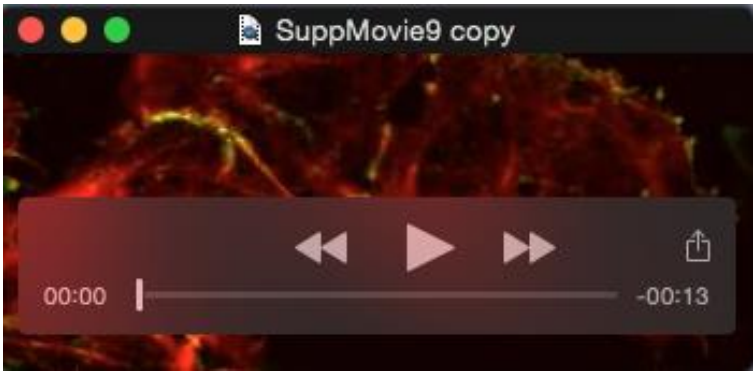

Movie 9. Confocal timelapse of cells in a St. 12 explant taken at 63x with a 5 second interval and playing at 8 frames per second. This explant was made from an embryo expressing both C-Cad:GFP and Life-Act:mCherry. Neighboring cells combine to make linear actomyosin and C-Cadherin adhesion structures that run across both cells. Note that at the same time as a cells are participating in the actin:C-Cad:actin structures that we hypothesize transmit tension across the tissue that the same cells can also express lamellipodial protrusions at different regions of their cell membranes. These Phase 3 cells exhibit a large, dense C-Cad plaque between them that are attached to actin filaments in both cells (bottom middle) and the center of this adhesion is displaced rapidly as the cells actively contract. Additionally, a large lamellipodia is protruding simultaneously and just adjacent to the large cadherin plaque, while the anterior face of the cell exhibits small filopodial “kiss points” with an unlabeled neighbor at the top of the screen, an apparent third distinct functional use of C-Cad in these cells. The C-Cad dynamics in each of these three behaviors shows the rapid nature of regulation the proximal actin activity has on C-Cad localization and clustering. Furthermore, a combination of all three of these behaviors can be expressed at the same time in cells undergoing MIB, likely based on local cues such as tension.

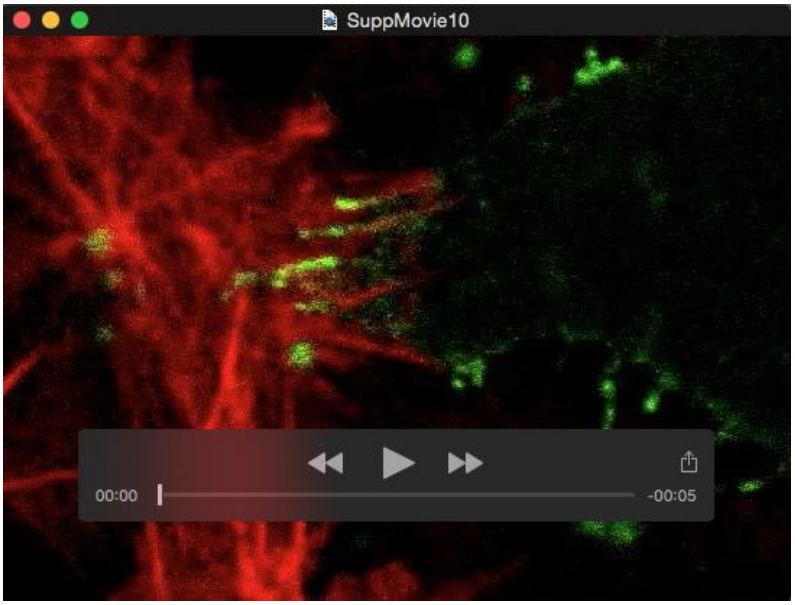

Movie 10. Confocal time lapse imaging of a St. 12 explant made at 150x, with a 5 second interval and playing at 8 frames per second. This explant was made from an embryo injected with C-Cad:GFP in one cell and LifeAct:mCherry in the other cell at 2-cell stage. C-Cadherin (green) and cortical actin (red) that are each singly expressed in closely associated neighboring cells mediate tissue adhesion in a tensile environment. In this movie, one cell makes an adhesion with its neighbor, revealing the relationship between C-Cad in one cell and cortical actin in another cell as they make a functional adhesion. In addition, a natural experiment occurs during this timelapse because the cell-to-cell contact visualized in this movie breaks for an unknown reason. This breakage results in a rapid retraction of the individual cells, consistent with the hypothesis these type of cell-cell contacts are under tension and supporting the idea that C-Cad is the adhesion molecule responsible for cell-on-cell traction during CE.

Movie 11. Confocal time lapse of a cell in a St. 12 explant at 90x, taken at a 5 second interval and playing at 8 frames per second. This explant is made from an embryo mosaically co-expressing C-Cad:GFP and LifeAct:mCherry in RLC morphant cells. RLC morphant cells exhibit both cytoskeletal and C-Cad localization defects during CE. The cytoskeleton does not progress past Phase 1 or 2, maintaining a basket around the periphery of the cell involving finely crosslinked bundles of actin. Lamellipodia that form exhibit rapid rearward flow and fail to establish proto-nodes. Additionally, the C-Cad on the lamellipodia does not establish discrete puncta, remaining a diffuse cloud of green signal at the distal end of the lamellipodia (compare to Movie 8).

Movie 12. Confocal time lapse of cells in a St. 12 explant at 63x, with a 5 second interval and playing at 8 frames per second. This explant was made from an embryo mosaically morphant for RLC, in a C-Cad:GFP and LifeAct:mCherry background. An RLC morphant cell (blue cell in Fig 6E) fails to establish and maintain C-Cad based adhesions with neighboring wild-type cells. As a wild-type cell extends a large lamellipodia onto the cortex of the morphant cell, there is little cooperation in adhesion from the morphant, resulting in retraction of the lamellipodia and apparent failure to make a functional adhesion. In contrast, the same wild-type cell can be seen making functional adhesions, based on the appearance on C-Cad puncta, with a different wild-type neighbor.

Movie 13. Confocal time lapse of cells in a St. 12 explant at 63x with a 5 second interval and playing at 8 frames per second. This explant was made from an embryo mosaically expressing pnRLC:mCherry and C-Cad:GFP in RLC morphant cells, Similar to RLC morphant cells alone (see Movie 12), morphant cells that are expressing pnRLC do not display protrusions with the same frequency as controls. However, rather than exhibiting large lamellipodia with a diffuse cadherin signal that do not appear to adhere as in RLC morphant cells (compare to Movie 11), the pnRLC expressing RLC morphant cells appear to maintain stable adhesions once established. This lack of adhesion remodeling would be expected to retard progression of MIB, resulting in defects in CE.